# Numerical study of dust plume impact on urban thermal comfort

Jérémy Bernard[1,2], Tim Nagel[1], Valéry Masson[1], Aude Lemonsu[1], Jean Wurtz[1], Pierre Tulet[3], and Quentin Rodier[1]

[1]Météo-France, CNRS, Univ. Toulouse, CNRM, Toulouse, France
[2]EDYTEM, CNRS, Le Bourget du Lac, France
[3]LAERO, CNRS, Univ. Toulouse, IRD , Toulouse, France

**Correspondence:** Jérémy Bernard (jeremy.bernard@zaclys.net)

**Abstract.** In Europe, heatwave conditions associated with southern synoptic flows can sometimes be combined with ~~dust plume events~~ episodes of dust plumes coming from the Saharian desert. ~~The aerosol plume modifies the~~ Change in the atmospheric composition of aerosols alters the radiation observed near the ground~~and consequently~~ , resulting in impacts on other variables such as air temperature. This study focuses on ~~a heatwave and its corresponding plume of Saharian dusts that have reached~~ the heatwave experienced by the Paris region from 15 to 19 June ~~2022.~~ 2022, combined with the passage of a Saharan dust plume. To investigate the aerosols impact on ~~the~~ local weather conditions and thermal comfort, three ~~numerical simulations based on the~~ Meso-NH ~~model~~ atmospheric numerical simulations are used: one without dust aerosol (C0), one with ~~CAMS dust data~~ dust aerosols defined from CAMS reanalysis (C1), and one with twice the concentration of CAMS dust ~~data~~ aerosols (C2). Simulation C1 is validated against observations from the PANAME-Urban experimental campaign. The ~~impact of aerosols on~~ time evolution of Aerosol Optical Depth and incoming solar radiation at the surface ~~are~~ is well reproduced, ~~and the~~ with improvement in the resulting air temperature and boundary layer ~~heights are improved when taking into consideration the aerosols. The presence of a dust plume during the heat wave contributes to reduce~~ height when taking aerosols into consideration. The radiative effect of dust aerosols results in a decrease in incoming solar radiation and air temperature ~~to~~ of up to 75 W ~~/m~~m$^{-2}$ and 1 ~~K~~°C, respectively. At 16 ~~:00 UTCin sunny places of urban and suburban areas~~UTC, it results in a thermal comfort improvement of up to 1°C in sunny urban and suburban areas. However, in ~~the shade of~~ shaded suburban areas, the increase ~~of diffuse radiation and relative air humidity as well as the decrease of~~ in diffuse solar radiation and humidity and the decrease in wind speed induced by the dust aerosols counterbalance the air temperature decrease, ~~thus leading to no improvement of the thermal comfort~~ resulting in no thermal comfort improvement.

## 1 Introduction

~~Atmospheric aerosols,~~ The frequency, intensity and duration of heat wave events are increasing over time and is expected to continue to increase due to climate change (**?**). Urban citizens, representing most of the world population, are facing even warmer events due to the urban local climate (Oke et al., 2017). The so-called Urban Heat Island (UHI), defined as the difference in air temperature between the city and its surroundings, can reach values up to 10 °C for large cities like Paris (**?**) and is expected to rise with rising air temperature (**?**). UHI is generally more pronounced at night but other variables are locally altered by urban settings. The mean radiant temperature, aggregating the radiant exchange with a human and its environment, is generally lower when the built areas is getting denser due to shadow generated by buildings (?). However, densely built areas are subject to lower wind speed due to the additional surface roughness created by the buildings (?).

The urban climate is impacted by atmospheric aerosols. For example, **?** have shown that the summer UHI in China is reduced due to higher aerosol concentrations in urban compared to rural areas. Indeed, atmospheric aerosols, including mineral dust, play a critical role in modulating weather and climate. As reviewed by sch and references therein, dust particles are formed through natural processes and can be transported from one continent to an otheranother, influencing atmospheric chemistry, radiation, and cloud microphysics. Their impacts are particularly relevant during large-scale dust outbreaks, which strongly modify surface and boundary layer conditions.

One of the mechanisms by which aerosols affect the atmosphere is through their interaction with radiation. Depending on their optical and microphysical properties, aerosols can scatter and absorb solar shortwave (SW) and longwave (LW) and long-wave radiation, thereby altering the surface and atmospheric energy budget. The use of an aerosol climatology for global models based on the tropospheric aerosol scheme shows an effect of up to 30 $W/m^2$ W $m^{-2}$ over desert, partly compensated by the increase of LW radiations (about 10 $W/m^2$ - wan)long-wave radiations (about 10 W $m^{-2}$, wan). Observational studies of a Saharan dust outbreak over Barcelona (Spain) confirm this level of magnitude: in June, Córdoba-Jabonero et al. (2021) documented that when the aerosol optical depth (AOD) reached 0.45 at 532 nm, the decrease in net SW solar radiation was 54 $W/m^2$ W $m^{-2}$ while the increase in net LW long-wave radiation was 11 $W/m^2$W $m^{-2}$. Similarly, at the end of May, **?** reported that including dust–radiation interactions in a simulation of a Saharan dust event in southwest Germany reduced the net SW solar radiation by up to 80 $W/m^2$ W $m^{-2}$ (for an AOD of 0.36).

These radiative perturbations directly affect the near-surface air temperature. **?** simulation reduced significantly (up to 1 K°C) the positive bias in the forecast of near-surface air temperature. During the 2003 European heatwave, characterized by AOD values between 0.4 and 0.6, numerical experiments with the Weather Research and Forecasting Model (WRF, Skamarock et al., 2005) indicated that aerosols reduced net SW solar radiation by 30–50 $W/m^2$W $m^{-2}$, corresponding to a 15% reduction in solar flux (per). This decrease in surface energy led to air temperature reductions of up to 0.3 K°C, consistent with other observational estimates observations (zha, a). Closer to the dust emission source, the impacts of dust aerosols can be more important: for a dust storm in West Africa, where the dust was located distributed over the boundary layer, the reduction in the near-surface air temperature reached 4 K °C (Tulet et al., 2008).

wan emphasizes that the vertical The type and the location of the aerosols are crucial. While the effect of some aerosols (such as sulfate or nitrate) is mainly limited to solar radiation diffusion, some others (black carbon for example) can also absorb the solar radiation and convert it into heat (?). In this case, the distribution of absorbing aerosols is crucial: heating near the surface can enhance entrainment in the planetary boundary layer (PBL), whereas heating aloft tends to stabilize the atmosphere by strengthening the inversion layer (wan). Thus, through their effect on radiation and surface near-surface air temperature, aerosols also exert strong control on turbulence, PBL dynamics, and wind fields. Reduced surface heating weakens turbulent mixing, leading to a shallower boundary layer and lower wind speeds. For example, per reported reductions in PBL height of 200 m (10%) and wind speed decreases of 1.2 m /ss$^{-2}$ (6%) in response to aerosol–radiation interactions. Observations by par further support this, showing wind speed reductions up to 20% when surface solar flux was suppressed by 200 ~~$W/m^2$~~ W m$^{-2}$ due to Asian dust layers.

Anthropogenic aerosols are among the largest sources of uncertainty in radiative forcing (sto). Mitigation policies have already demonstrated a reduction of the aerosols concentration (Hodnebrog et al., 2024). Thus, the trend being at adding more stringent mitigation policies to improve air quality, aerosol emissions are likely to be reduced worldwide during the 21st century. zha (b) ~~have~~ investigated the effect of the projected aerosol decrease on the worldwide increase of intensity, frequency, and duration of ~~heat waves~~heatwaves. Their results show that future ~~green house~~ greenhouse gases increase will result in future (2081–2100) heatwaves that are, when globally averaged over land, significantly more intense (+2.4 ~~K~~ °C on average air temperature), longer (17 days) and more frequent (12 more heat wave days per year), compared to present-day. These changes will also be further aggravated by aerosol reductions, leading to an increase of ~~their~~ the mean intensity, length and frequency of heat waves by 0.6 ~~K~~°C, 7 days, and 2 more days per year, respectively.

Although there is a quite dense scientific literature showing the impact of aerosols on near-surface atmospheric variables, most of ~~them~~ the simulations are performed at coarse resolution (12 km to 36 km - ber and per, respectively) and ~~, to the best of the authors knowledge, none~~ very few are dedicated to ~~evaluate the impact on~~ explore the effect on urban climate, more specifically on human thermal comfort. ~~More specifically, urban areas, where most of the population is concentrated, are already impacted by their local climate (Oke et al., 2017) and might be directly affected by the presence of large amounts of aerosols in the atmosphere.~~ **?** have simulated the effect of urban haze on solar radiation and boundary layer meteorology but they have not analyzed their results in the scope of modification of the urban thermal comfort. **??** have explored the aerosol effect on the UHI intensity. However, the focus was mainly performed on night-time and some thermal comfort key variables such as mean radiant temperature were not considered. On the contrary, **?** have investigated the role of aerosols on the mean radiant temperature for a person located in the middle of a building block street but they do not consider the effect of the aerosols on air temperature, wind speed or relative humidity. Moreover, they have only performed their calculation for a person, exposed to the sun, at noon, while during heat events, pedestrians are more willing to stay in shadow areas. Indeed, the shadow provided by buildings can be seen as cool places during clear days (Masson et al.) but these areas might be affected by the interactions between aerosols and radiation in the atmosphere. To study how the aerosol concentration can impact thermal comfort in urban areas, we simulate a heatwave event in the Paris region associated with an inter-continental Saharan dust outbreak using an atmospheric model coupled with an urban surface model at a resolution of 1.2 km.

## 2 Material and method

### 2.1 Meteorological overview

The present study focuses on the heatwave ~~period that strokes~~ that strucked the Paris region from 15 to 19 June 2022. The ~~synoptic overview of this event~~associated synoptic conditions, based on the ERA5 reanalysis (Hersbach et al.), ~~is~~ are presented in Fig. 1. The air temperature at 850 hPa in the Paris region gradually ~~warms up~~ warmed to 20°C from 15 to 18 June under the influence of a 500 hPa cut-off located west of Portugal ~~that generates advection of~~ and advecting hot air from ~~North~~ Northern

Africa and the Iberian Peninsula toward France. In addition, a high geopotential at 500 hPa ~~grows over Franceleading to air subsidencefurther increasing~~ developed over France, causing air subsidence, which further increased the near-surface air temperature. The 850 hPa ~~temperature warms~~ air temperature rose until 18 June, which was classified as a notable heat peak day by Météo-France and the national Public Health Agency (~~under rev.~~in pressLemonsu et al.~~under rev.~~in press). This ~~episode~~ heatwave ended on the night from 18 to 19 June, as the low-pressure system moved northeastward, bringing cooler oceanic air over France and leading to ~~important rainfall and~~ heavy rainfall and air temperature drop over the Paris region.

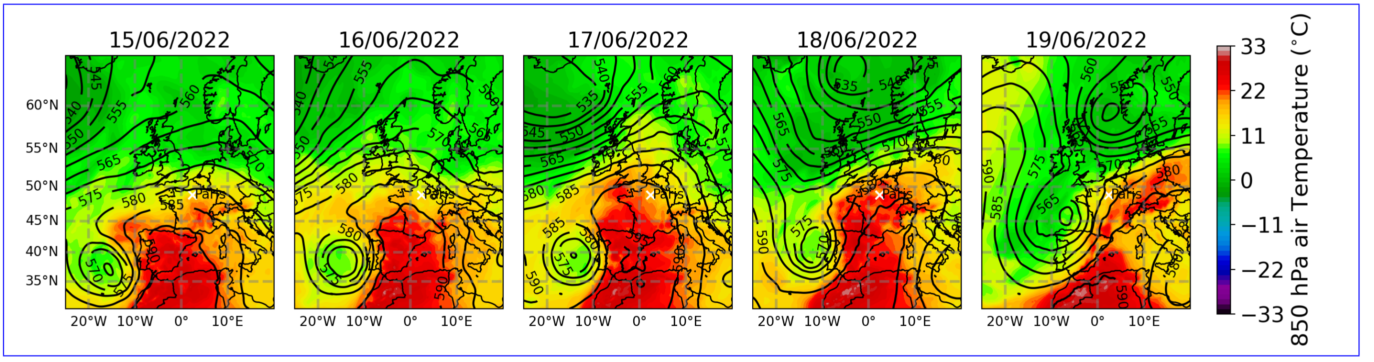


**Figure 1.** Synoptic overview at 12 ~~:00~~ UTC (14 LT) from 15 to 19 June 2022 based on ERA5 reanalysis (Hersbach et al.). The ~~colours~~ colors and the contours represent the air temperature at 850 hPa and the 500 hPa geopotential height, respectively.

~~This heat episode was not only remarkable because it was the earliest ever recorded heatwavein France, but also because a Saharan dust event outbreak occurred simultaneously, driven by the strong southerly flow. The dust AOD~~ During this heatwave, the strong southerly flow caused a significant transport of Saharan dust that affected a large part of France, including the Paris region. The time series of dust AOD maps at 550 nm, based on the ~~CAMS reanalysis (Rémy et al., 2022), is mapped from 15 to 19 June 2022 in~~ Copernicus Atmosphere Monitoring Service Integrated Forecasting System (CAMS-IFS, Rémy et al., 2022) (Fig. 2~~. The dust plume reaches~~ ), shows that the dust plume reached the Paris region in the afternoon of 16 June and ~~begins to leave it on~~ left from 19 June, as the low-pressure system ~~moves~~ moved northeastward. Note that ~~observations derived from ground ceilometers in the Paris region~~ the vertical profiles of aerosol backscatter coefficients from ground-based remote sensing measurements obtained during the PAris region urbaN Atmospheric observations and models for Multidisciplinary rEsearch(PANAME-Urban ~~under rev.~~in pressLemonsu et al.~~under rev.~~in press) experimental campaign show that before 17 June~~the~~, the dust aerosols were in the troposphere (not shown), so interactions with aerosols in the boundary layer was not possible before this date.

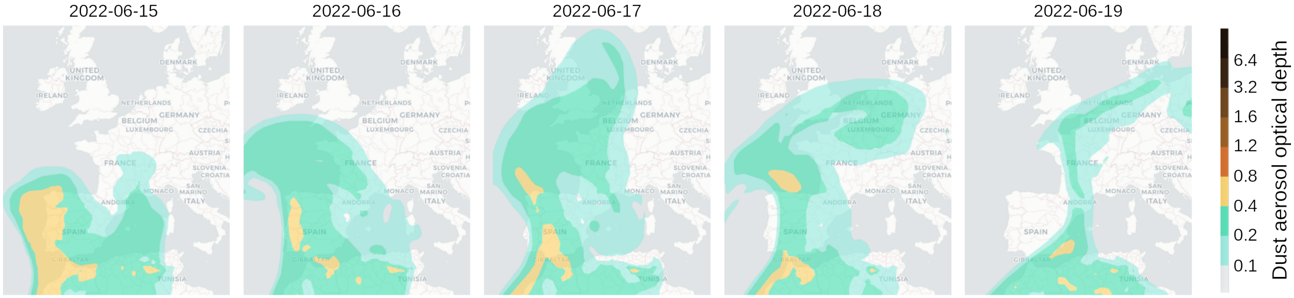


**Figure 2.** Dust aerosol optical depth (550 nm) every day at noon from 15 to 19 June 2022 based on ~~CAMS reanalysis~~ CAMS-IFS (Rémy et al., 2022). ~~Source: Dust~~ The figure is adapted from data and ~~/or~~ images ~~were~~ provided by provided by the World Meteorological Organization (WMO) Barcelona Dust Regional Center and the partners of the Sand and Dust Storm Warning Advisory and Assessment System (SDS-WAS) for Northern Africa, the Middle East and Europe.

The ~~CAMS data, used~~ dust AOD from CAMS-IFS, whose reanalysis (Inness et al.) serves as input for this study, ~~are compared with other dust data sources at the Palaiseau station location~~ is compared with the total AOD measured by ground-based sun photometer located in Palaiseau at the SIRTA (Site Instrumental de Recherche par Télédetection Atmosphérique ?) observatory (∼20 km southwest of Paris) ~~in Fig. 3. The models have been chosen to highlight the variability of the AOD values: SILAM (sof) has the minimumAOD values, ZAMG-WRF-CHEM (leg) the maximum~~ and with the dust AOD multimodel forecasts (minimum, ~~while MULTI-MODEL, a multi-model ensemble(bas) can be seen as median values. For this period , the~~ maximum and median (called MULTI-MODEL, bas), based on 16-model ensemble) provided by the Barcelona dust regional center plat-form (Fig. 3). For the period considered, CAMS-IFS ~~(Rémy et al., 2022)~~ is quite close to the ~~MULTI-MODEL~~median value simulated by the models. The observations ~~have an offset of~~ of total AOD show a shift toward higher AOD values by about 0.1 compared to models, which is particularly visible on the first two days. This offset is due to the model AOD ~~definition,~~ limited to dust particles. Nevertheless, and despite a large spread of the ensemble, ~~while the observations are affected by all types of aerosols. From the end of 16 June and until 19 June,~~ the temporal ~~variability~~ evolution of the AOD from 16 to 18 June is well represented by ~~all the models: there is an increase of the~~ the models, with an increase in AOD during the night from 16 to 17 ~~night~~June, a slight decrease ~~during~~ on 17 June~~and the highest values~~ , and peak values reached during the next night and day. ~~Only the SILAM data does not have clear higher AOD values on 18 June.~~ However, there is a large variability in terms of AOD intensity, the simulated dust AOD on 18 June ranging between 0.1 ~~in SILAM~~ and up to 0.5~~in ZAMG-WRF-CHEM~~. The variability of the AOD values between the data source can be ~~part ly~~ partly attributed to their quite large spatial resolution difference, from 0.2° for ~~ZAMG-WRF-CHEM and SILAM~~min and max models, to 0.75° for ~~CAMS~~CAMS-IFS.

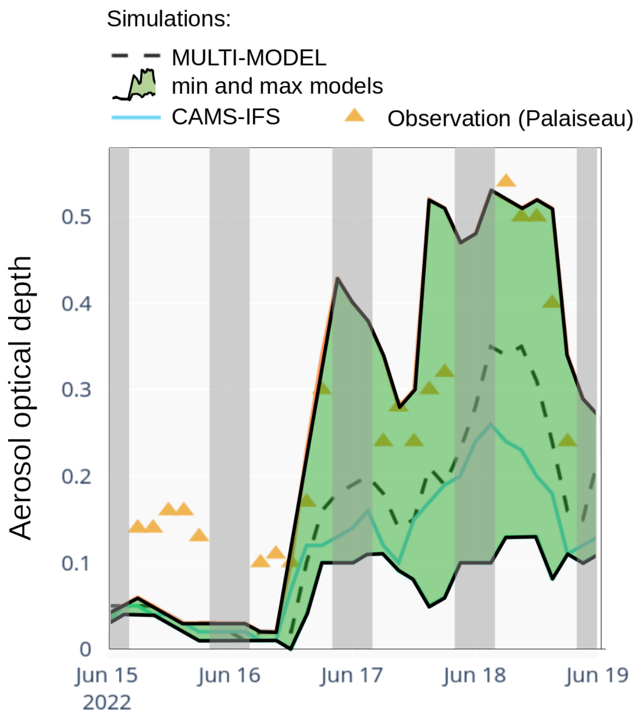


**Figure 3.** Aerosol optical depth at 550 nm from 15 to 19 June 2022. The observation is the total aerosol optical depth at the Palaiseau station while the model data ~~is~~ only represents the effect of the dust aerosols. The ~~choice of the~~ min, max and MULTI-MODEL models ~~was performed in order to~~ illustrate the variability ~~of~~ and the median dust AOD values ~~: ZAMG-WRF-CHEM, CAMS-IFS, SILAM and MULTI-MODEL.~~ of the 16 models proposed on the Barcelona Dust Regional Center plat-form. The figure is adapted from data and ~~/or~~ images ~~were adapted from~~ provided by the WMO Barcelona Dust Regional Center and the partners of the Sand and Dust Storm Warning Advisory and Assessment System (SDS-WAS) for Northern Africa, the Middle East and Europe. Here and for the other figures in the manuscript, the shaded gray time period correspond to nighttime.

### 2.2 Model ~~and Numerical experiments~~description

#### 2.2.1 Atmospheric model

In this study, the non-hydrostatic research atmospheric model Meso-NH (Lac et al., 2018) is coupled with the SURFace Externalised ~~Land Surface Model (SURFEX, Masson et al., 2013)over a single 480 km by 480 km domain of 1.2 km horizontal resolution, covering the northern part of France and centered on Paris (Fig. 4).~~ land surface modeling system (SURFEX, Masson et al., 2013 . For the wind advection, a third-order weight essentially non-oscillatory scheme (WENO3) is used and combined with a five-stage third-order Runge-Kutta time-splitting scheme (**?**). The ~~model time step is set at 5 seconds. The~~ atmospheric turbulence scheme, based on a prognostic equation for the turbulent kinetic energy (**?**), only accounts for vertical turbulent fluxes and is closed with the mixing length of Honnert et al. (2021). Deep convection is explicitly resolved while shallow convection is parameterized with an Eddy-Diffusivity-Kain-Fritsch scheme (**?**). The historical radiative solver of Meso-NH is used: the Rapid Radiation Transfer Model (Mlawer et al., 1997) for ~~LW~~ long-wave radiation is coupled with a ~~SW~~ short-wave scheme based on the Fouquart (1980) method. Finally, microphysics is solved using the ICE3 one-moment scheme (Pinty and Jabouille, 1998; Riette; Wurtz et al., 2023).

### 2.2.2 Dust scheme

The transport of desert aerosols and the evolution of their size distribution are described by three log-normal modes according to the Organic Inorganic Lognormal Aerosol Model (ORILAM, Tulet et al.). These modes are initialized using CAMS reanalysis (Inness et al.) of size distribution with median diameters of 78 $nm$, 0.64 $\mu m$, and 5 $\mu m$, and respective standard deviations of 1.75, 1.76, and 1.70 (**?**). Radiative properties (extinction, single scattering albedo and asymmetry factor) are computed on-line using the method described by **?** and are coupled to the six wavelength bands of the **?** radiation scheme.

### 2.2.3 Surface model

Surface physics is handled by ~~the last version of SURFEX (~~SURFEX V9.0~~), and the~~ .0, according to four main cover types with dedicated surface schemes (sea and ocean, inland water, natural soil and vegetation, and urban). The component fraction of the ~~four tiles~~ cover types per grid cell is ~~given by the ECOCLIMAP-SG~~ derived from the ECOCLIMAP-Second Generation land cover database ~~(Wiki – CNRM, 2018). Each tile~~ (ECOCLIMAP-SG, Wiki – CNRM, 2018). Each cover type uses a dedicated scheme to calculate the fluxes over the surface. For urban ~~tiles~~areas, the multilayer version of the ~~TEB~~ Town Energy Balance (TEB) urban canopy model (Masson, 2000; Schoetter et al., 2020) is used, allowing the buildings to interact directly with the first atmospheric layers using a drag approach and releasing fluxes at the corresponding atmospheric model levels. In-canyon urban vegetation and street trees are also taken into account (Redon et al., 2017, 2020). For rural and natural tiles, the ~~Soil-Biosphere-Atmosphere interaction~~ Interaction Soil–Biosphere–Atmosphere (ISBA) land surface model ~~(Noilhan and Planton, ISBA)~~ (Noilhan and Planton) is used, with an explicit multi-layer soil approach to model water and heat vertical transfers (**?**). The ~~ISBA~~ Multi-Energy Budget parameterization ~~(Boone et al., 2017, MEB) is used, allowing to model~~ is activated in ISBA (ISBA-MEB, Boone et al., 2017) to deal with a low and high vegetation canopy that is separated from the ground.

~~Currently, Meso-NH is coupled with the explicit CAMS aerosol data. However, due to the large variability of AOD values obtained in the various models used to predict dusts (Fig. 3)~~

### 2.2.4 Thermal comfort

The TEB model, described in Sect. 2.2.3), computes inline the Universal Thermal Climate Index (UTCI, **?**). The UTCI is a bioclimatic index that describes the physiological comfort of humans under specific meteorological conditions. It is expressed as a temperature (in °C). Following **?**, its operational procedure calculation is based on an equation involving four meteorological variables: air temperature ($T_a$, ~~three simulations are performed: i) C0 uses the dust concentration set to 0,~~

~~ii) C1 uses the CAMS data as input,~~ °C), mean radiant temperature ($T_{mrt}$, °C), relative humidity ($RH$, %) and wind speed ($U_{wind}$, m s$^{-1}$). Equation (1) shows that UTCI can be calculated as the air temperature plus an offset that depends on all the aforementioned variables (**?**):

$$\mathrm{UTCI} = T_a + \mathrm{Offset}(T_a, U_{wind}, T_{mrt}, RH) \tag{1}$$

TEB computes the UTCI for a person located in the middle of the urban canyon and exposed to the incoming short-wave (direct and diffuse components) and ~~iii)C2 uses twice the CAMS data values as input.~~

~~Except for dust data,~~ long-wave radiation, to the ~~numerical configuration for these three simulations is identical and adapted from other studies of the PANAME-Urban framework (Forster et al., 2024under rev.~~in press~~; Lemonsu et al.under rev.~~in press~~)~~ ~~.~~ short- and long-wave reflected radiation inside the canyon, and to the infrared radiation emitted by the surrounding walls and ground surfaces (**?**). In TEB, $T_a$, $RH$, $T_{mrt}$, and $U_{wind}$ are calculated at 1 m, 1 m, 1.1 m and 10 m above ground level (AGL), respectively. To provide a sub-grid information on UTCI variability related to sun-shade contrasts, TEB computes two UTCI diagnostics, one for a person standing in the sun (by considering all radiation contributions) and one for a person in the shade (by excluding direct radiation contribution).

### 2.3 Numerical experiment

The model is run with a 1.2-km horizontal resolution over a 480 km by 480 km domain, covering the northern part of France and centered on Paris (Fig. 4). The vertical grid is divided ~~in~~ into 68 levels with a first half-level at 2 m AGL for physical variables such as air temperature. The grid size increases along the vertical, with a constant stretching of 1.17 up to 1000 m and 1.04 above. The domain extends vertically up to approximately ~~17,500~~ 17500 m. The maximum vertical grid size allowed is 500 m. A simulation consists of a single 4-days Meso-NH run with a 5 seconds time step.

The ~~amount of dust aerosols is set according to the CAMS global reanalysis (Inness et al.) . It is provided as~~ objective of the study is to investigate the effect of desert dust aerosols on urban thermal comfort. Thus, only dusts are explicitly coupled with Meso-NH, the level for the other aerosol types (black carbon, organic and sulfate-type, and sea-salt aerosols) being taken from the Tegen et al. (1997) climatology. To account for the "actual" changes in dust aerosol concentrations in the atmosphere during the simulation (in response to the passage of the Saharan plume), the dust aerosol data from the CAMS reanalysis (Inness et al.) are provided to MesoNH with a 3-hour timestep. To test the sensitivity of the simulation to the dust aerosols, three simulations are performed: i) C0 sets the dust concentration to 0, ii) C1 uses the concentrations from CAMS data as input, and iii) C2 doubles the concentrations from CAMS data.

The CAMS reanalysis provides a concentration in ~~$\mu g/m^3$~~ dust aerosols in $\mu$g m$^{-3}$ for each cell of 0.75° by 0.75° ( ~~80 km by 80 km~~ 73 km by 111 km at this latitude) with 35 vertical layers within the model domain extension. The inclusion of CAMS aerosols into the Meso-NH model is prone to uncertainties. The total mass content given by CAMS is distributed according to log-normal modes that can be described by the 0th, 3rd, and 6th moment of the distribution (**?**Hoarau et al.). Assumptions are made on the shape of the distributions of aerosols, which influence the radiative properties. Note that for simplification, only dust transport ~~is~~ and dry dust deposition are included in the simulations~~. Due~~ : due to the short period of simulation and the fact that the aerosols are outside of the boundary layer, the modification of the dust aerosols content by wet deposition, aggregation or chemical reaction is not simulated. ~~For all non-desertic types of aerosols, in each simulation, the Tegen et al. (1997) six-class aerosol climatology is used.~~

~~Each simulation (C0, C1 and C2) consists of a single 4-days Meso-NH run. The~~

For all simulations, the initial conditions for the atmospheric and surface fields, as well as the atmospheric boundary conditions, come from the ~~AROME-France analysis (Seity et al.; Brousseau et al.), which includes data assimilation~~ analysis output of the french numerical weather prediction model AROME-France (Application of Research to Operations at Mesoscale, Seity et al.), which uses a three-dimensional variational (3DVar, Brousseau et al.) data assimilation scheme and is also coupled with SURFEX. Data assimilation is not performed directly in Meso-NH.

### 2.4 Observation network

The simulations ~~presented~~ described above can be compared with numerous meteorological observations, distributed over the Ile-de-France administrative region (which includes Paris). The measurement types and their ~~location~~ locations are shown in Fig. 4 and described hereafter.

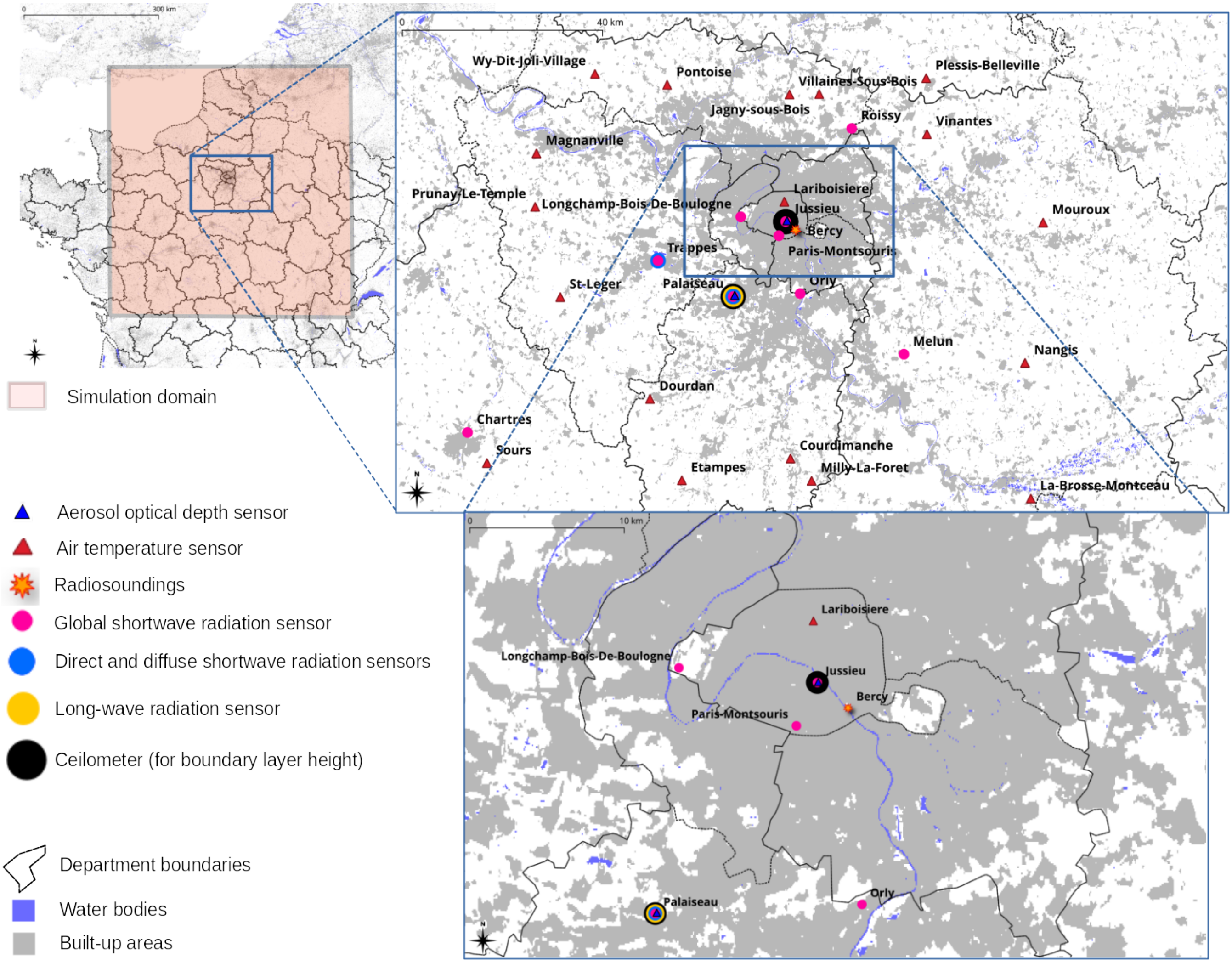


**Figure 4.** Representation of the model configuration and observation network. ~~©OpenStreetMap contributors 2025. Distributed under~~ Built-up areas and water bodies are derived from the ~~Open Data Commons Open Database License (ODbL) v1.0~~map produced by ?.

The AOD ~~, for wavelengths included~~ for wavelengths between 340 and 1640 nm ~~,~~ is observed by two ~~AERONET stations (hol): one~~ AErosol RObotic NETwork (AERONET) stations (hol). One is located in ~~the~~ Jussieu (center of Paris) and the second ~~is at Palaiseau .~~in Palaiseau (blue triangles in Fig. 4).

The Météo-France permanent surface network ~~(RADOME, Tardieu and Leroy)~~ (Radome, Tardieu and Leroy) has nine automatic weather stations (AWS) located nearby Paris that ~~have global SW radiation sensors.~~ record global solar radiation (purple dots in Fig. 4). Two of them also record direct and diffuse ~~SW~~ components of solar radiation (Trappes and Palaiseau), and one record the ~~LW~~ long-wave radiation (Palaiseau).

Comparing atmospheric model simulations with observations of 2 m AGL air temperature in cities is not straightforward, due to the lack of representativeness of AWS stations (Oke et al., 2004). Indeed, to follow the recommendations of the World Meteorological OrganizationWMO recommendations, AWS operated by national meteorological services should be installed in large and homogeneous areas of flat terrain and low-rise vegetation. Finding sites Locations that match these constraints is particularly complex are complex to find in or near urban areas, which as these areas are characterized by a quite high land cover heterogeneityand thus far from the standard large area of grass vegetation. Thus, in suburban areas, the stations are often AWS are generally located in small patches of low-rise vegetation areas in airports, and, in cities, they are often located in urban parks. Because, in In the present study, the model grid mesh grid mesh of the model is 1.2 km. Therefore, a single cell often includes both urban and rural land cover types. This is particularly remarkable in or nearby large urban areas. Although , this is particularly true in Paris or in its suburbs. As a consequence, although the observation station is located in a low-rise vegetation area of 200-500 m wide, the grid cell will simulate model will calculate fluxes released by the low-rise vegetation area but also by a large amount of urbanized surfaces, making the comparison impossiblebetween simulations and observations non-relevant. To prevent this inconsistency, only a sample of all the RADOME stations located in the study area is chosen: 17 stations defined as 'rural ' in-situ stations where the corresponding model grid cell surface cover matches their immediate surroundings are used for the air temperature evaluation. This results in 18 rural stations and a unique station defined as 'urban ' urban station (Lariboisière) are selected. All 'rural ' stations have less than 20% of their surface covered by urban features (the urban fraction is calculated as a bilinear interpolation of the urban fraction of the four closest grid cells) while the 'urban' , see Fig. 4). The rural stations are located away from Paris, whereas the urban site is located in a non-vegetated part of Paris city center and the model cell where it is located being 100% urban . (i.e. the surface fluxes in the corresponding model cell are calculated only with TEB). In the model, because of the 1.2 km resolution, suburbs have often a mix in surface cover between rural and urban features. Therefore, in-situ suburban stations of the Radome network are excluded from the comparison.

The air temperature of the upper atmosphere is observed using radiosondes measurements released from the Bercy (?, inner part of Paris(location called Radiosoundings in , near the Seine River - Fig. 4). The atmospheric boundary layer height is also estimated from two ceilometers, located in Jussieu (near the city center) and Palaiseau, using the algorithm described by Kotthaus et al. (2020). Note that more details on each instrument can be found in the description of the PANAME-Urban experimental campaign (under rev.in pressLemonsu et al.under rev.in press).

## 3 Results

The simulations without dust (C0) and with CAMS dust aerosols (C1 and C2) are compared with the observations on first compared to observations in the Paris region to assess the quality of the simulations, as well as the impact of aerosols on radiation and air temperature. Then, the effect of aerosols on the thermal comfort during the heatwave thermal comfort is investigated in SeeSect. 3.4. In the followingsections, if not specified, the simulated data refers to the simulation simulation results refer to C1.

### 3.1 Aerosol optical depth

According to Fig. 5, the AOD simulated by C1 and observed in the Paris region agree ~~well. For both observations and simulations, the aerosols start to affect the~~ relatively well (Pearson correlation coefficients is on average 0.58, 0.86 and 0.86 for C0, C1 and C2 respectively, with p-values much lower than 0.01). A comparison of the AOD times series observed at Palaiseau station and simulated at the corresponding grid cell shows that the dust aerosols cause a sharp increase in AOD on the afternoon of 16 June, ~~the maximum AOD being~~ that peaks on 18 June~~while~~. On 15 June~~is the day with the lowest AOD mean~~, prior to the arrival of the Saharan plume, background AOD values were much lower. Figures 5a-c show that the higher the wavelength, the lower the AOD but also that for all wavelengths, the increase ~~of~~ in AOD between 15 and 18 June is nearly the same (about 0.3). ~~Last, the AOD difference between the location of the two nearby AOD stations (Paris and Palaiseau are~~ Lastly, the small differences in AOD noted between Jussieu (urban) and Palaiseau (suburban) stations, located about 20 km apart ~~-~~ (Fig. 4)~~is low (<~~, with variations of less than 0.07 for observations and ~~<~~0.05 for simulations ~~)~~(not shown here), indicate that the effect of dust aerosols prevails over that of local urban aerosol sources.

However, differences are also observed. First, there is a small negative bias (about −0.1) of the simulated AOD ~~. This bias is not constant over time, even when there is no dust plume , *i.e.*, on~~ on 15 ~~June. This~~ June, when the dust plume have not yet reached our study area. This bias may be due to the use of a climatological value for ~~all non-desertic aerosols with~~ aerosols other than dust. Indeed, in the Tegen et al. (1997) climatology, ~~whose~~ aerosol values are expected to be representative of a monthly mean ~~,~~ and may underestimate their concentration~~during clear sky heatwave conditions. Concerning the dust plume, the AOD increase (on 16 June) and decrease (on~~. Except on 17 June, the level of magnitude of this daily mean bias remains constant over time for the C1 simulation. The level of aerosols being maximum on 18 June~~) is much sharper in the observation than~~, this day is considered as the more interesting to observe the effect of aerosols on the meteorological variables near the surface. The sharp variations in observed AOD related to the passage of the dust plume are smoothed in the simulation, which is probably explained by the low horizontal resolution of the initial field provided by the CAMS data ~~. Also, and contrary to the three other days, the observed AOD on 17 June is lower than the simulated one. For this reason, the effects of the aerosols on the surface variables are expected to be more accurately simulated on 18 June (especially morning)than on 17 June~~( 73 km by 111 km at the Paris latitude).

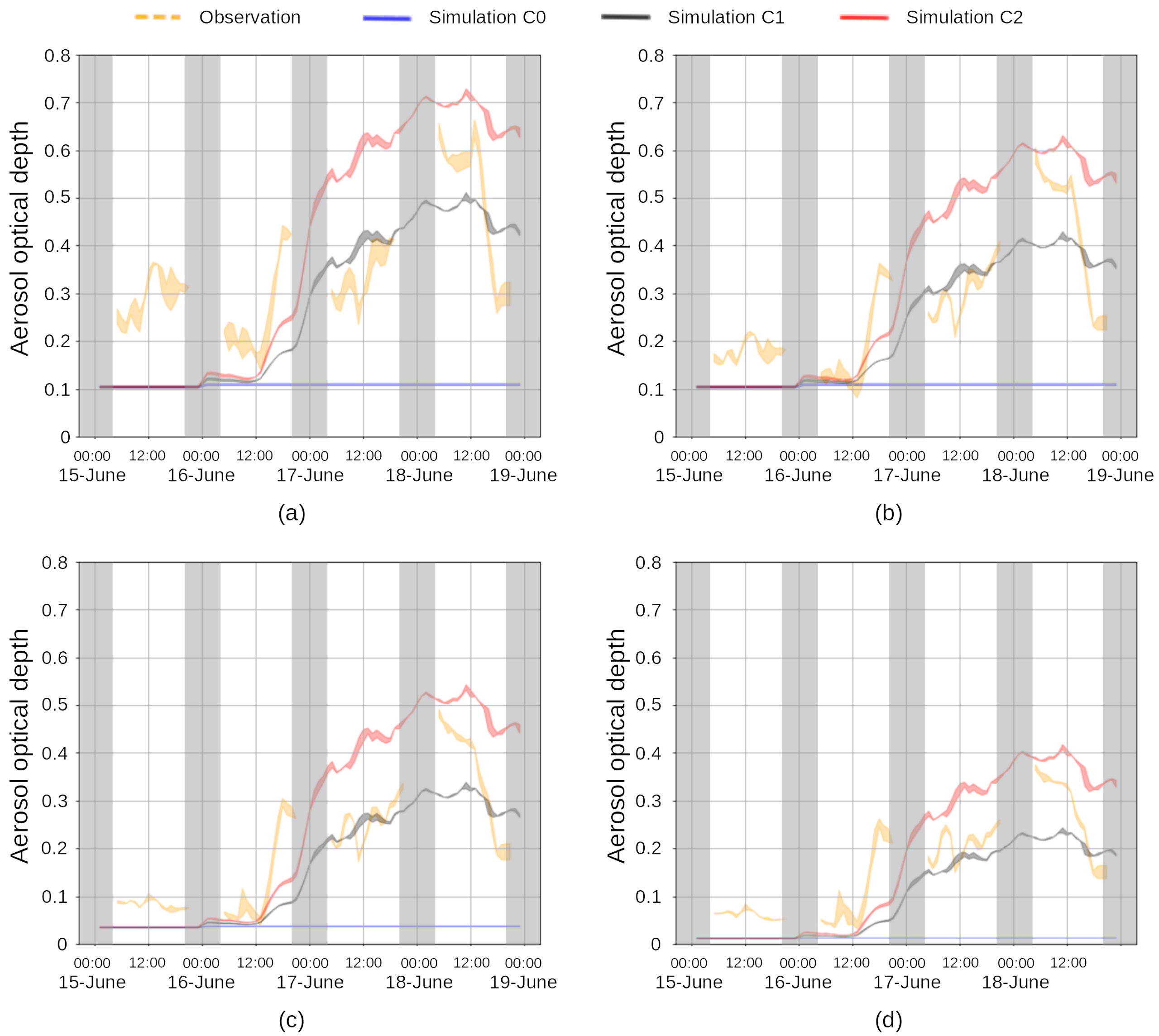


**Figure 5.** ~~The~~ Time-series of aerosol optical depth observed (and simulated) at the Palaiseau station (a) at 340 nm (250-440 nm), (b) at 500 nm (440-690 nm), at 1020 nm (690-1190 nm) and (d) at 1640 nm (1190, 2380 nm). Note that this is not possible to observe AOD during night-time (20 UTC to 04 UTC).

## 3.2 Radiation

The ~~4-days~~ heatwave event investigated ~~includes a day without dust plumebut~~ begins on 15 June, one day and a half before the dust plume, with a partially cloudy sky~~(15 June)~~, followed by ~~3~~ three days with increasing dust aerosols above the Paris region. ~~These~~ This evolution of atmospheric conditions affect the global ~~downward solar radiation: on~~ solar radiation. On 15

June, the observed and simulated data show a signal shape and maximum intensity altered by the clouds, both in Chartres (Fig. 6a) and in Roissy (Fig. 6b). On the afternoon of 16 June, the ~~aerosol cloud~~ dust plume reaches the Paris region from the ~~South-West~~south-west, affecting the ~~Western~~ western part of the region (Fig. 6a) more than the ~~Eastern~~ eastern one (Fig. 6b).

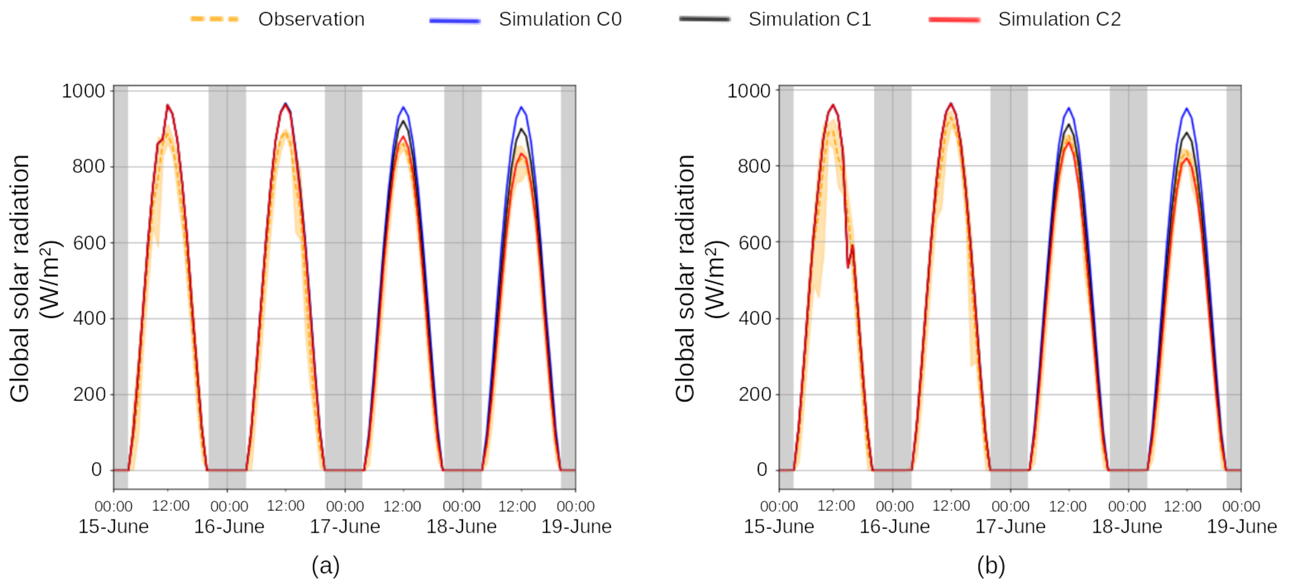


**Figure 6.** The global ~~downward~~ solar radiation (a) in Chartres, the most ~~Western~~ western radiation station, and (b) in Roissy, the most ~~Eastern~~ eastern radiation station. Note that the observation ~~line~~ curve is ~~the hourly average value and is surrounded by a patch~~ delineated at the bottom and at the top by the hourly minimum and maximum, respectively.

For the first two days, ~~where~~ there is a limited amount of aerosols in the atmosphere ~~, the simulation overestimates the observed radiation~~and no significant differences between C0, C1 and C2. However, all simulations overestimate the observed incoming solar radiation with a larger bias on 15 June. This could be caused by ~~the presence of contrails~~ contrails in the morning and sparse cumulus humilis ~~on the 15 June morning and afternoon respectively (not shown),~~ in the afternoon that are not ~~simulated by the model~~present in the simulations (not shown). The underestimation of ~~the non-desertic AOD (~~AOD for aerosol other than dust (see Sect. 3.1) could also contribute to this bias. ~~However, while there is a general negative offset of the simulated AOD, the AOD increase between 15 and 18 June is nearly the same for simulations and observations (see Sect. 3.1). Therefore, to~~ Therefore, in order to quantify the mitigation of incoming solar radiation by dust and evaluate the ability of the model to simulate ~~the effect of the increase of dust aerosols on global radiation, the global radiation from~~ this effect (while eliminating the model's inherent biases), Fig. 7a shows the diurnal cycle of solar radiation on 15 June~~is subtracted that of~~ , subtracted from those on 17 and 18 June ~~(Fig. 7a). The nine in situ AWS equipped to measure radiations are used to produce this figure in order to illustrate the spatial variability of the effects.~~ in both observations and simulations, for the nine measurement locations (purple dots in Fig. 4). On 17 June, ~~the~~ C1 ~~simulation~~ overestimates the effect of ~~the~~ aerosols, which is consistent with the AOD overestimation shown in Sect. 3.1. On 18 June, ~~the~~ C1 ~~simulation~~ performs well in the morning~~with~~

an effect of , mitigating the global solar radiation up to 75 W /mm$^{-2}$ in the simulation versus compared to 65 W /mm$^{-2}$ in the observations. However, during During the afternoon, the effect of the aerosols on the global solar radiation mitigation effect is again highly overestimated (by about 30 W /m$^2$ offset). Again, this is understandable looking at the m$^{-2}$ that is explained by the different dynamics of AOD (Fig. 5): in the afternoon, the the observed AOD drops very quickly from noon while it decreases very slowly in the simulations, leading to a large overestimation of the simulated AODan increasing offset. Note that the spike in the simulations occurring in the afternoon is due to the presence of clouds in the Eastern eastern part of the region during the reference day (15 June - Fig. 6b). Overall, on 18 June, Despite the identified shortcomings, the daily mean effect of the aerosol on global radiation has mitigation of global radiation on 18 June is of the same order of magnitude between the simulation C1 (-32 W /m$^2$) and the observations ($-32$ W m$^{-2}$) and observations ($-25$ W /m$^2$ - Tab. m$^{-2}$, as shown in Table 1).

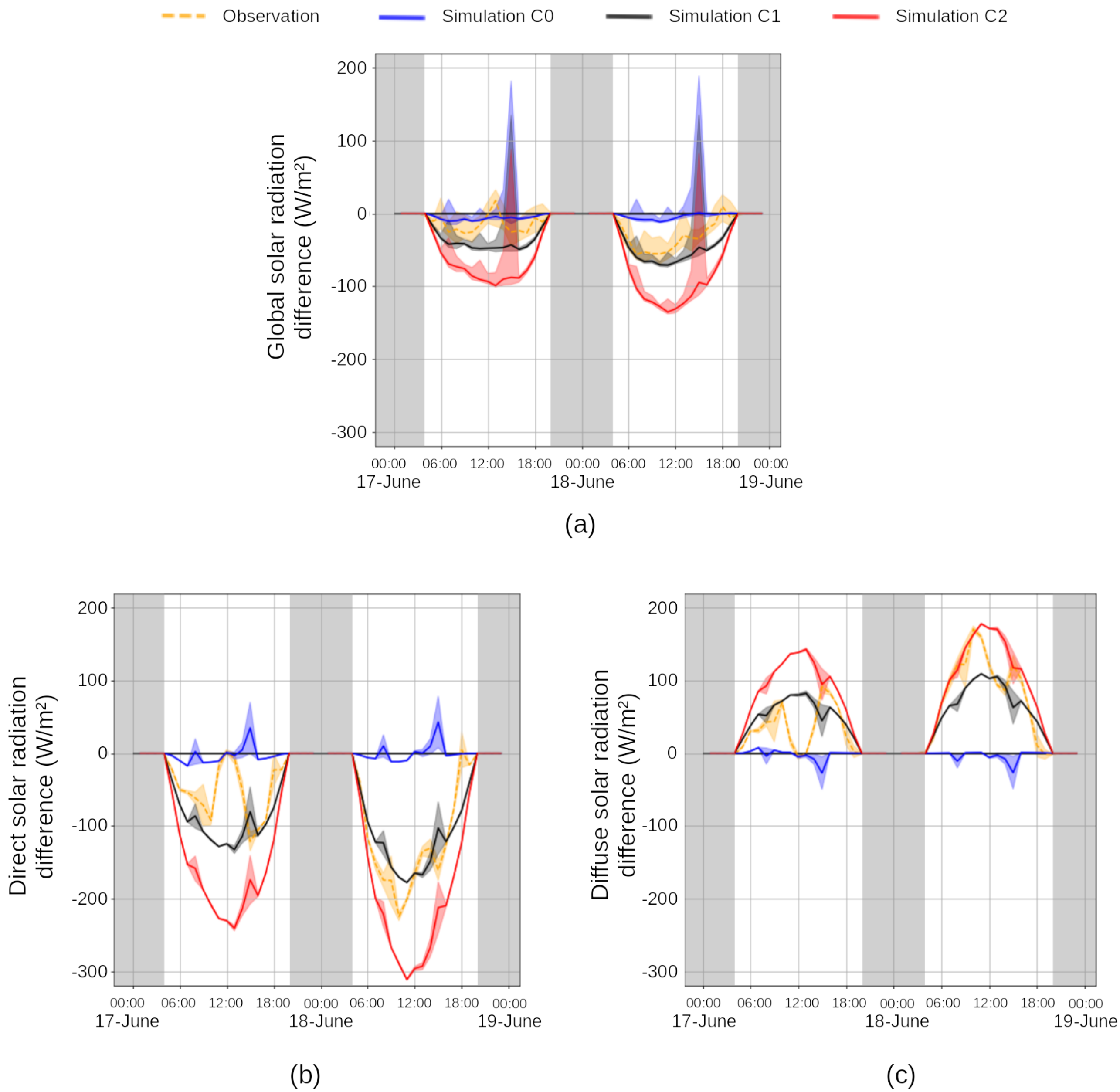


**Figure 7.** (a) ~~global~~Global, (b) direct and (c) diffuse ~~downward SW~~ solar radiation difference for 17 and 18 June compared with 15 June. The mean value of the nine (two) global (direct and diffuse) ~~SW~~ solar radiation stations is represented by the ~~line~~ curve and is surrounded by a patch delineated at the bottom and at the top by the 0.1 and 0.9 quantiles, respectively.

~~Although the simulations slightly underestimate the direct radiation decrease and the diffuse radiation increase, the effect of the aerosol on the solar radiation share between~~ The attenuation of global incoming solar radiation is accompanied by a change in the direct and diffuse radiation is rather accurately simulated for 18 June (components due to the optical properties of dust particles. This effect is illustrated in Fig. 7band Fig. 7c). Again, the sudden late morning peak for both direct and diffuse observed solar radiation is attributable to temporary clouds ,c using radiation data from Jussieu and Palaiseau. On 18 June, the partitioning of global radiation in C1 underestimates the diffuse component in the late morning period when temporary clouds are observed on 15 June (reference day). Otherwise, the diffusive effect of dust is quite well simulated by C1. The observed effect is more important than the one simulated by C1 and less important than the one simulated by C2.

The daily mean SW and LW radiation averages of global solar radiation and long-wave radiation are compiled in Table 1. For the reference day (15 June), they have the same order of magnitude (between 340 and 380 W /$m^2$ Tab. 1350 and 346 W $m^{-2}$ for observations) but the average error of simulation mean bias for C1 is slightly higher for the daily SW solar radiation (+16 W /$m^2$) than for the daily LW (-2.5 W /m19 W $m^{-2}$ against $-5$ W $m^{-2}$ for long-wave). However, the effect of dust aerosols on the daily mean downward infrared long-wave radiation is minor (-3 W /m$-3$ W $m^{-2}$ between C1 and C0 on the 18th), which makes these long-wave impacts impacts of long-wave negligible compared with solar radiation reduction (-31 W /m$-31$ W $m^{-2}$).

**Table 1.** The daily average global solar radiation (W /$m^{-2}$) and long-wave radiation (W $m^{-2}$) observed and simulated at the Palaiseau station for the reference day and the daily anomaly average, corresponding to the difference between a given day and the reference day. The numbers in brackets are the difference of solar radiation between a day simulation and the observations for the reference day (15th 15 June)

| | | 2022-06-15 Daily average (bias) | 2022-06-16 | Daily anomaly avera |
|---|---|---|---|---|
| | | 2022-06-17 15 June (REF) | 2022-06-18 17 June | 18 June |
| Global solar radiation (W $m^{-2}$) | Observation Obs | 350 (0) | 352 (2) $-12$ | 338 (-12) 325 (-25) |
| | C0 | 369 (0+19) | 371 ($-2$ ) | 367 (-2) 368 (-1) |
| | C1 | 369 (0+19) | 370 (1) $-24$ | 345 (-24) 337 (-32) |
| | C2 | 369 (0+19) | 369 (0) $-46$ | 323 (-46) 309 (-60) |
| Long-wave radiation (W $m^{-2}$) | Observation Obs | 346 | 340 +17 | 363 383 +37 |
| | C0 | 341 (-5) | 341 +26 | 367 378 +37 |
| | C1 | 341 (-5) | 341 +24 | 365 375 +34 |
| | C2 | 341 (-5) | 341 +23 | 364 373 +32 |

## 3.3 Air temperature

### 3.3.1 Near ground Near-ground air temperature

The comparison of near-ground Comparison of near-surface air temperature is performed for the 17 'rural ' 18 rural sites and for the single 'urban ' urban site. When there is no aerosol plume are no dust aerosols in the atmosphere (15 June), the air temperature of almost all simulated by the model for urban and rural stations is overestimated by the model in the afternoon underestimated from 06 to 12 UTC (00 - 06 UTC being the spin-up time it is not considered) and overestimated the rest of the day (about 1.75 K) but performs very well during the night (°C for the rural median value - Fig. 8a). When explicitly considering the presence of aerosols, the model overestimation decreases in the afternoon for all simulations (on 18 June , the median error raises up to 5 K for C0 against 4 For the night between 15 and 3 K for C1 16 June (20 UTC - 04 UTC) the bias is close to zero. The daytime (from 04 UTC to 20 UTC) warm bias increases in rural areas on 17 and C2, respectively). The night-time simulated air temperature is also affected by the presence of aerosols: at midnight on 18 June, the median error is +2 K, +1.5K and +1 K as temperatures rise, but differently depending on the simulations : it is maximum for C0 , C1 and (without dust aerosols) and minimum for C2 , respectively. The same simulation error dynamic is observed for the urban station (by doubling CAMS dust aerosols). Although trends are quite similar at the urban site for the three simulations (Fig. 8b). ,d), biases are lower. A warm nighttime bias with similar distinction between the simulations appears on 17 and 18 June for urban and rural stations.

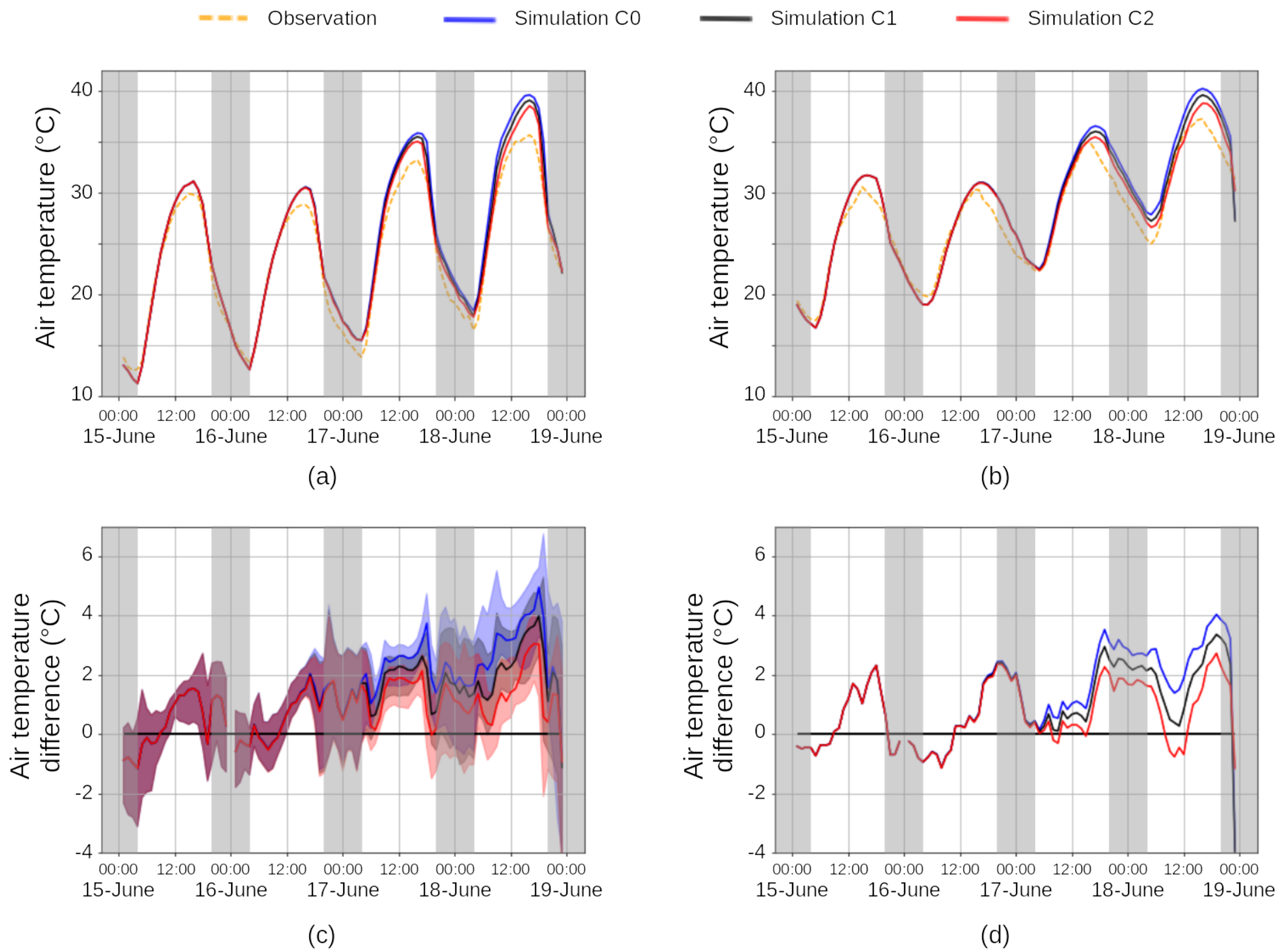


**Figure 8.** (a) Observed and simulated ~~absolute~~ air temperature and (c) difference between simulation and observation for rural stations. (b) Observed and simulated ~~absolute~~ air temperature and (d) difference between simulation and observation for the urban station. For rural stations air temperature differences, the median value of the 18 stations is represented by the ~~line~~ curve and is surrounded by a patch delineated at the bottom and at the top by the 0.1 and 0.9 quantiles, respectively.

As ~~for the~~ with solar radiation, the ~~distinction between~~ air temperatures in the simulations with and without aerosols ~~starts~~ start to diverge on 17 June~~and increases afterward~~, and this difference increases on 18 June. Overall, ~~when aerosols are considered in the simulations, it~~ taking aerosols into account clearly improves the ~~performance of the model for the~~ simulation of the near-surface air temperature~~throughout the simulation period. More specifically, on the second half of the morning of 18 June, the C1 simulation difference with observation is nearly the same (about 0.5 K) as during the morning of 15 June (day without aerosol). This suggests that the effect of the aerosol on the air temperature (about 1 K decrease) is well simulated by the model. In the next section~~. In Sect. 3.3.2, the vertical structure of the atmospheric boundary layer is ~~further investigated~~

~~to identify~~ investigated to understand the reason for the ~~near-ground~~ air temperature bias ~~of the model~~near the surface, more specifically the afternoon overestimation.

### 3.3.2 Upper atmosphere air temperature

The ~~evaluation of the~~ impact of dust aerosols on the vertical ~~thermal structure of the~~ stability of the first 6000 m of the atmosphere can be ~~undertaken~~ assessed by comparing the ~~simulation results with data from~~ simulations with each other and with radiosonde and ceilometer measurements. ~~The focus is on~~ Figure 9 shows the vertical profiles of potential air temperature[1] recorded by radiosondes released from Bercy on 18 ~~June, during which four weather radiosondes were released from the inner part of Paris:~~ June at 00~~:00~~, 12~~:00~~, 16~~:00~~, and 20 ~~:00 (Fig. 9).~~ UTC (see location in Fig. 4).
At 00 ~~:00 UTC~~ UTC (Fig. 9a), the urban boundary layer (UBL) is well mixed~~and its~~ . Its height is well captured by all the simulations~~. The UBL~~ , but its air temperature is slightly too warm~~, as in the residual layer~~ . This is also the case for the residual layer above it up to 1000 m~~. This is likely remaining from the overestimation of the previous day air temperature~~ , probably resulting from a warm bias on the previous day (17 June, not shown). Above 1000 m, in the free atmosphere, the simulated profiles of ~~temperature are similar and very good~~ potential air temperature are very similar and in good agreement with observations.

At 12 ~~:00 UTC~~ UTC (Fig. 9b), the differences in incoming solar radiation at the surface lead to different boundary layer heights between simulations. The best boundary layer simulation here is C2. The C0 boundary layer ~~height~~ grows twice faster, while C1 ~~is in the middle~~gives intermediate results. This shows that the dust aerosols have a significant effect ~~on~~ at this stage of the boundary layer development~~at this stage. During the afternoon~~ . At 16 UTC (Fig. 9c), all three simulations ~~produce a huge~~ largely overestimate the vertical development of the boundary layer ~~, contrary to the observations where the boundary layer extend remains limited, with a strong inversion~~ and underestimate its inversion strength. The turbulence and thermal ~~schemes~~ scheme used by the Meso-NH model probably simulate a too strong entrainment rate at the top of the boundary layer~~or a slight temporal shift in the simulations~~ , which could reduce the stability barrier in the free atmosphere. This could also be related to a slight time lag in the simulation of the large-scale structure change of the air mass that occurs in the evening~~, which could reduce the stability barrier in the free atmosphere~~. This strong entrainment causes ~~the extra heating~~ additional warming of the boundary layer and ~~the surface~~ surface during the afternoon (Fig. 8)~~during the afternoon. The simulations then overestimate the air temperature in the boundary layer~~, due to ~~this too high~~ excessive vertical extension of the boundary layer, resulting in ~~the incorporation of~~ mixing with warmer air from ~~above. The 18 June afternoon is the period with the largest disagreement between the simulations and the observations. Still, there is an~~ the upper layers. However, the comparison of the three simulations highlights the important role of the surface solar radiation reduction (due to the dust plume) in the dampening of the boundary layer development. At midnight (Fig. 9d), the nocturnal boundary layer ~~reforms, and~~ develops again, and air temperature differences between simulations are driven by the afternoon ones.

[1] The potential air temperature is defined as the temperature that the parcel would attain if adiabatically brought to a standard reference pressure (1,000 hPa); the calculation is made considering the air as an ideal gas

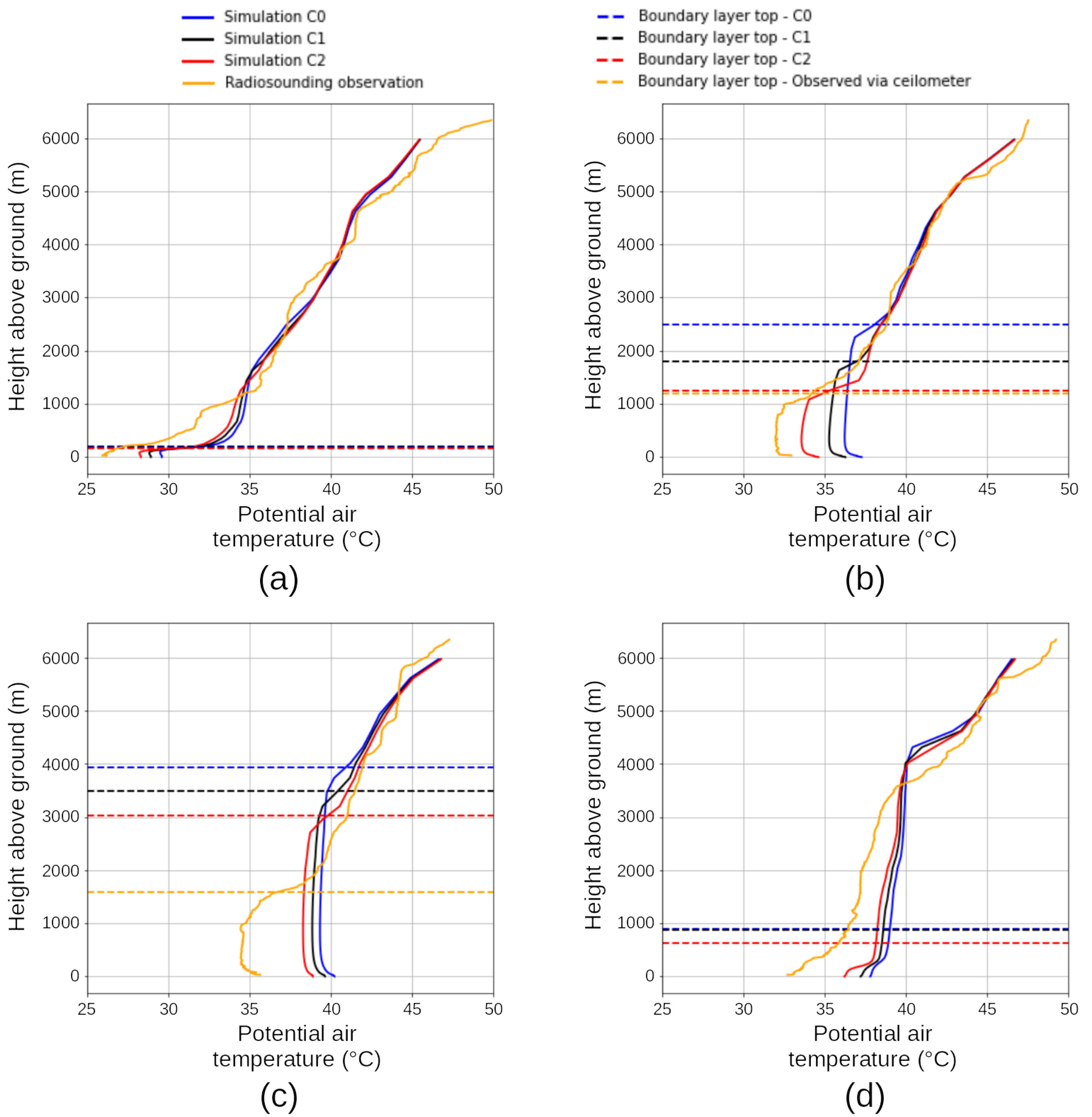


**Figure 9.** ~~Potential~~ Vertical profile of the potential air temperature ~~profile~~ simulated ~~at~~ by the ~~Jussieu station~~ Meso-NH model and observed ~~using~~ by a radiosonde at the Jussieu station location on 18 June at (a) 00~~:00~~, (b) 12~~:00~~, (c) 16 ~~:00~~ and (d) 20 ~~:00~~ UTC terms

.

~~The~~ In addition, the temporal evolution of the vertical structure of the first 4500 m of the the atmosphere during the ~~3~~ three days of the dust event is shown in Fig. 10. The model overestimates the boundary layer height ~~(observed by the Jussieu station ceilometer)~~retrieved from the ceilometer at the Jussieu station, but this is improved in C1 ~~simulation~~ compared to C0. ~~Comparison of the~~ The evolution of the difference in potential air temperature ~~observed with the simulations at the Jussieu station~~ between C1 and C0, vertically and as a function of time confirms previous findings: ~~for~~ taking dust aerosols into account in C1 ~~, during the two days with significant dust plume (17 and 18 June), there is~~ results in a cooling of typically 0.5°C ~~in the entire~~ throughout the boundary layer compared to ~~the simulation without dust~~C0 on 17 and 18 June.

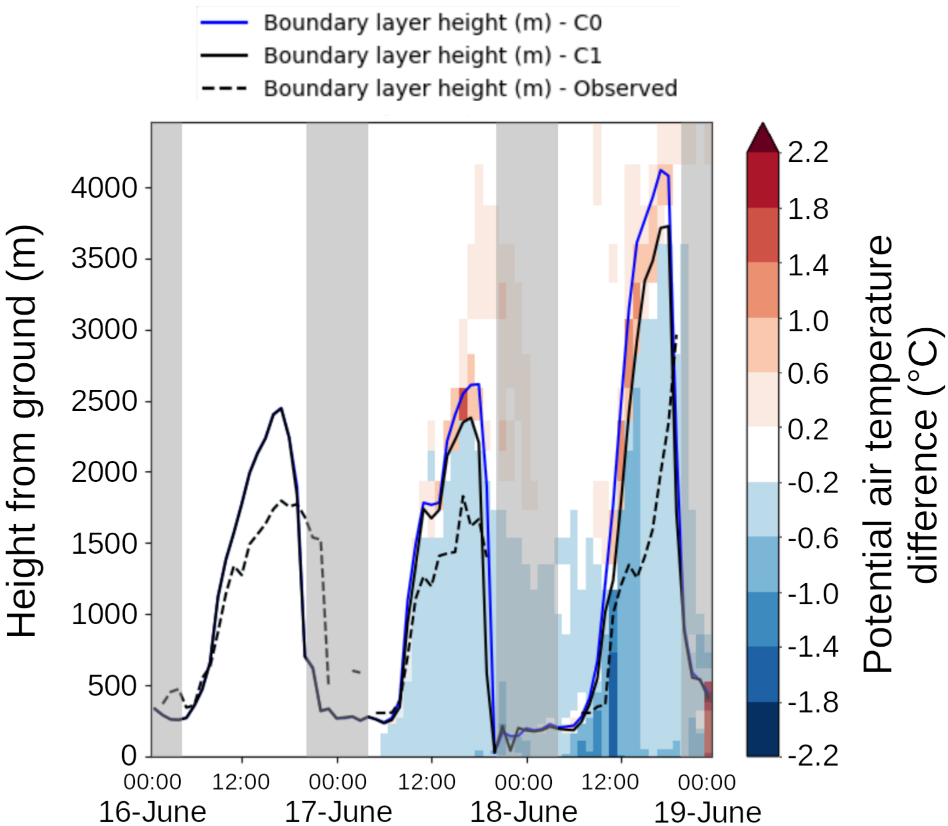


**Figure 10.** ~~Vertical~~ Comparaison of time-series of boundary layer height simulated (C0 and ~~temporal~~ C1) and observed at the Jussieu station, and vertical variation of the potential air temperature difference between ~~simulation~~ C1 and C0 at the ~~Jussieu station~~the same location

.

### 3.4 Thermal comfort

~~The effect of~~ In previous sections, the effect of dust aerosols on individual meteorological variables has been investigated. In the present section, we analyze the spatial and temporal variations of the UTCI bioclimatic index (see Sect. 2.2.4), which aggregates the effect of several meteorological variables on human thermal comfort. Previous results suggest that the C1 simulation is the one that catches the best the effect of aerosols on thermal comfort in urban areas is now being investigated. Previous sections showed that the effect of the aerosol on global, direct, and diffuse solar radiation was well predicted by simulation C1 (Sect. 3.2). The absolute values of both air temperature near the ground and boundary layer height were also improved when using this simulation (Sect. 3.3.1 and 3.3.2 respectively). Even if differences between observations and simulations remain, as for air temperature in the afternoon, we suppose that (Fig. 7). However, the near-surface air temperature is closer to the observation with C2 (Fig. 8). This is probably due to the fact that Meso-NH overestimates the entrainment at the top of the boundary layer, causing extra heating near the surface (Fig. 9). Increasing the aerosol quantity in the atmosphere, as done in C2, reduces the radiations reaching the surface, and therefore partially compensates for this bias, but this remains unrealistic. Moreover, the differential effect of dust is of the correct order of magnitude, in particular because the radiation forcing impact is well simulated (section 3.2). To illustrate the effect of this specific dust aerosol event on thermal comfort, the Universal Thermal Comfort Index (UTCI, Jendritzky et al., 2012) is calculated for simulations C0 and C1 and compared. The UTCI is a bioclimatic index that describes the physiological comfort of humans for specific meteorological conditions. It is expressed as a temperature and its calculation is based on an equation involving four meteorological variables: air temperature ($T_a$), mean radiant temperature ($T_{mrt}$), air relative humidity ($RH$) and wind speed ($U_{wind}$). Equation (1), shows that UTCI can be seen as the air temperature plus an offset which depends on all variables (**?**):

$$\mathrm{UTCI} = T_a + \mathrm{Offset}(T_a, U_{wind}, T_{mrt}, RH)$$

is known to be the main variable responsible for the spatial and temporal variability of human thermal comfort (**?**). Thus, only C0 (without dust) and C1 (considered as the most realistic one regarding radiation) are used for this section.

Fig. 11a and Fig. 11

Figures 11a,b show the UTCI calculated with TEB on 18 June simulated by for C1, for a person standing within the urban canyon in the sun and in the shade, respectively . The (see Sect. 2.2.4). The distinction between sun and shade is made because the mean radiant temperature, a very important driver for daytime outdoor thermal stress (**?**), is substantially reduced by shadow patterns created by obstructing objects such as buildings (**??**). The results are averaged for the time period from 15 :00 to 17 :00 UTC . The choice of this time period is motivated by the fact that UTC (17 to 19 LT). This choice is justified by two reasons: it is the warmest period of the dayand a large number of people in France usually move from their workplace to their homeduring this time slot. hottest time of day, and it is also the preferred time for commuting from work to home. The effect of aerosols on UTCI dust aerosols on thermal comfort is investigated by calculating the UTCI difference between C1 and C0 both in the sun and in the shade (Fig. 11c and Fig. 11d, respectively). The increase of in dust aerosol concentration in the atmosphere results in a slight decrease in UTCI values for the entire study area, although some contrasts are found: the decrease is more pronounced in the sun and in the city center (about −1°C) than in the shade and in the suburbs (about 0°C).

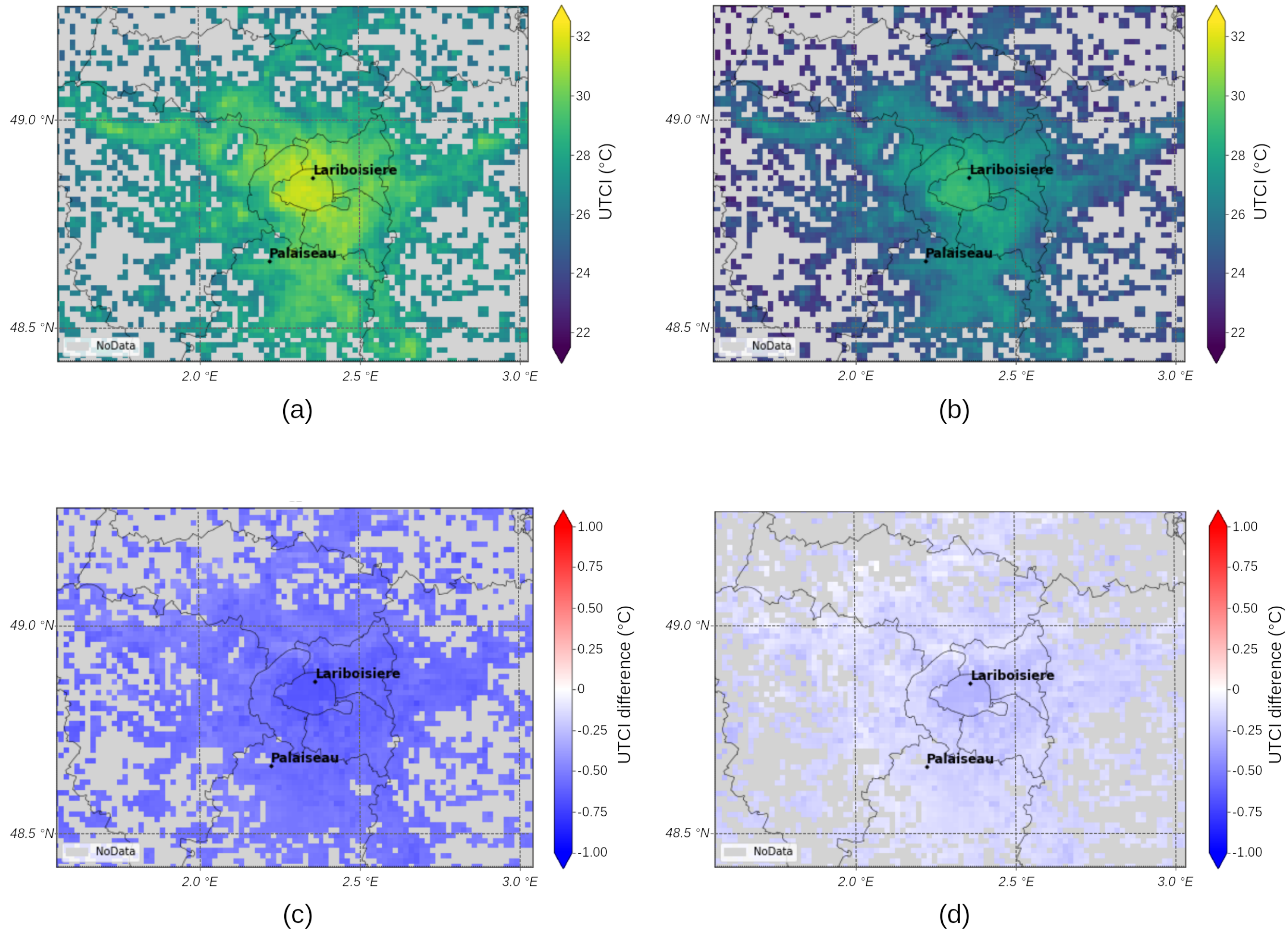


**Figure 11.** UTCI simulated bioclimatic index calculated by TEB on 18 June for the C1 in sun simulation, for a person standing within the urban canyon: (a) and in shade the sun and (b) in the shade. Difference between simulations C1 and C0 in the sun (c) and in the shade (d). All plots The results are from 18 June and averaged for the time period from 15 :00 UTC to 17 :00 UTC (17 to 19 LT). Missing data correspond to rural grid cells where the surfaces fluxes are calculated with ISBA only and therefore where no UTCI can calculated by the model

As shown in Sect. 3.3.1, the presence of dust aerosols decreases The contribution of the near-surface air temperature for all stations located in the study area. The contribution of this variable to UTCI can be removed in order to focus only on the UTCI offset term in the (Eq. 1. Then the results are more contrasted : the effect of aerosol is still negative in the sun (). The differences in UTCI offset in the sun and in the shade between C1 and C0 show more contrasted results than looking at differences in total UTCI (Fig. 12a,b). In the sun, the dust aerosols reduce the UTCI offset everywhere (city center and suburbs) (Fig. 12a)while it has a null or positive impact (up to 1.5. This is consistent with the reduction in the mean radiant temperature in the sun between C1 and C0, ranging from 1 to 3°C ) everywhere in the shade over the domain (Fig. 12b). The mean radiant temperature does not fully explain the effect of aerosol in the shade, as its effect is negative c). This is likely due to the increase in AOD that reduces the direct solar radiation at the surface, as described in **?** for several eastern Asia cities. However, in the shade, dust aerosols increase the UTCI offset in the suburbs (+0.5°C), but have a negligible effect in the city center (Fig. 12b). In the mean time, $T_{mrt}$ under shade is reduced in the dense urban area (Paris city center, see Fig. 12d) while having a null UTCI offset (Figbut slightly increase in the suburbs (+0.5°C). This increase is likely due to the increase in diffuse solar radiation (Fig. 6). However, the contrasting trends in $T_{mrt}$ and UTCI offset in the city center (Figs. 12b). In this specific area,d) suggest that the other variables play a role.In the city center, the slight decrease in wind speed (Fig. 12e) and the increase in relative humidity (Fig. 12f) compensate for the radiation effectare likely compensating for the decrease in mean radiant temperature. The decrease in wind speed has been previously documented in aerosol impact studies (per) and is attributable to the decrease of turbulence in the shallower boundary layer, while the . The increase in relative humidity is the result of both the explained by the decrease in air temperatureand a moister boundary layer (which did not incorporate much dry air through entrainment). On 18 June, , but also by an increase of the specific humidityof the . The difference in humidity between C1 simulation shows slightly higher values than the and C0 simulation (up to reaches its maximum at 16 UTC i.e. +0.4 g /kgof air at 4 pm, 0.2 g /kgat 10 am). kg$^{-1}$ of increase compared to the reference conditions of C0 (8.0 g kg$^{-1}$ on average). These more humid conditions near the surface in C1 results from the lower boundary layer height with less entrainment of dry air from upper layers.

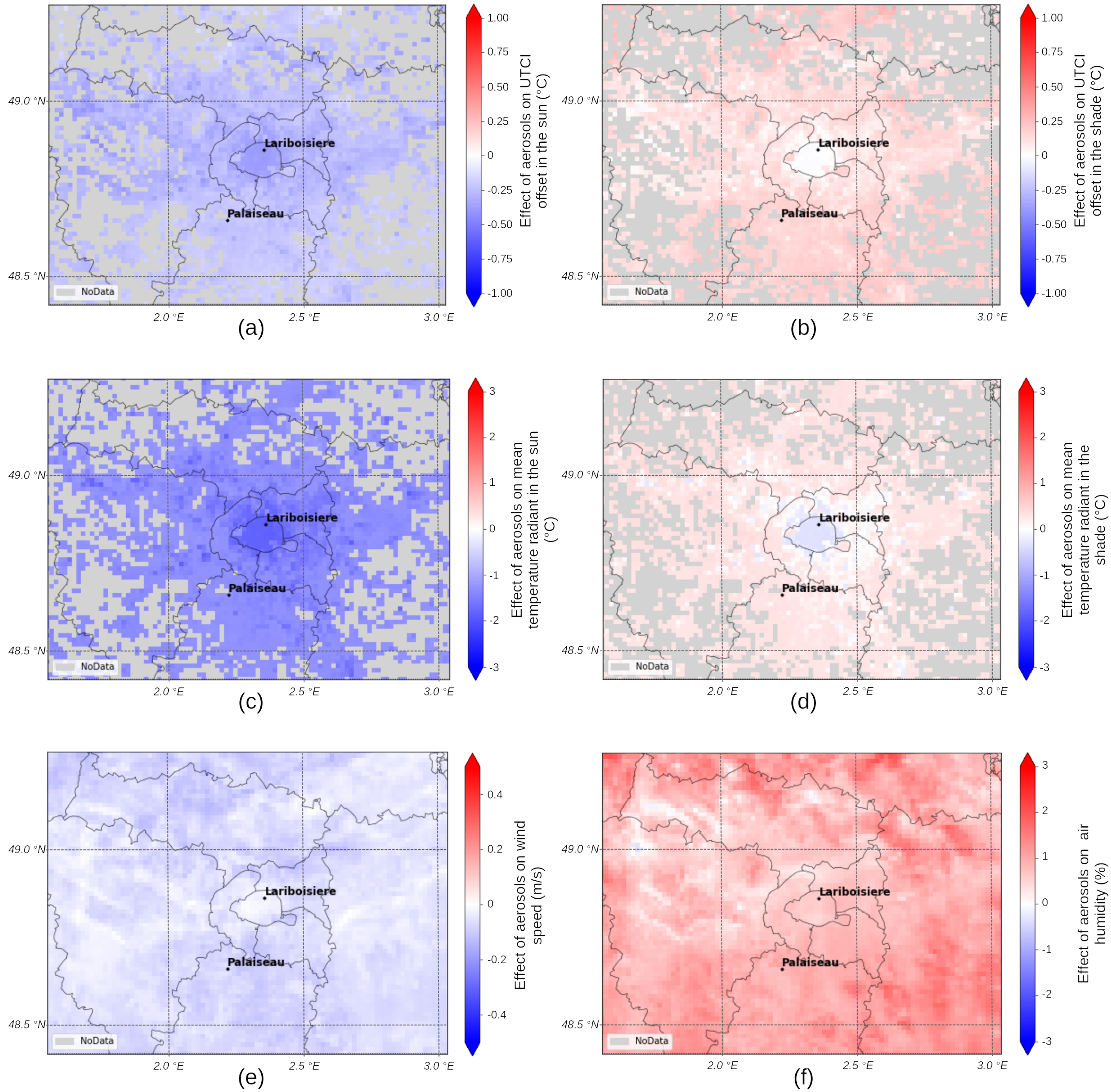


**Figure 12.** Difference between ~~simulations~~ Meso-NH C1 and C0 simulations for the UTCI offset (a) ~~UTCI offset~~ in sun ~~,~~ and (b) ~~UTCI offset~~ in shade, the mean radiant temperature (c) ~~$T_{mrt}$~~ in sun ~~,~~ and (d) ~~$T_{mrt}$~~ in shade, (e) wind speed and (f) relative humidity. All plots are from 18 June and averaged from 15 UTC to 17 UTC. Missing data correspond to rural grid cells where the surfaces fluxes are calculated with ISBA only and therefore where no UTCI can calculated by the model

Two stations located in different environments are were chosen to illustrate the temporal variability of the UTCI : offset from 15 to 18 June: i) the Lariboisière and Palaiseau station, located in a dense and non-vegetated urban environment within the city of Paris ; ii) the Palaiseau station, a suburban site with grass and sparse and low-rise buildings (see their location in Fig. 4). Lariboisière is the urban station. Its environment is composed of compact mid-rise buildings (Local Climate Zone (LCZ) type 2 - Stewart and Oke). Palaiseau, located south-west of Paris, includes many instruments. Its immediate environment is composed of sparse buildings (LCZ type 9). Note that the definition of each site is given using station environment is given based on aggregated spatial information using the from 1.2 km resolution grid cells.

Regardless of a person's location (

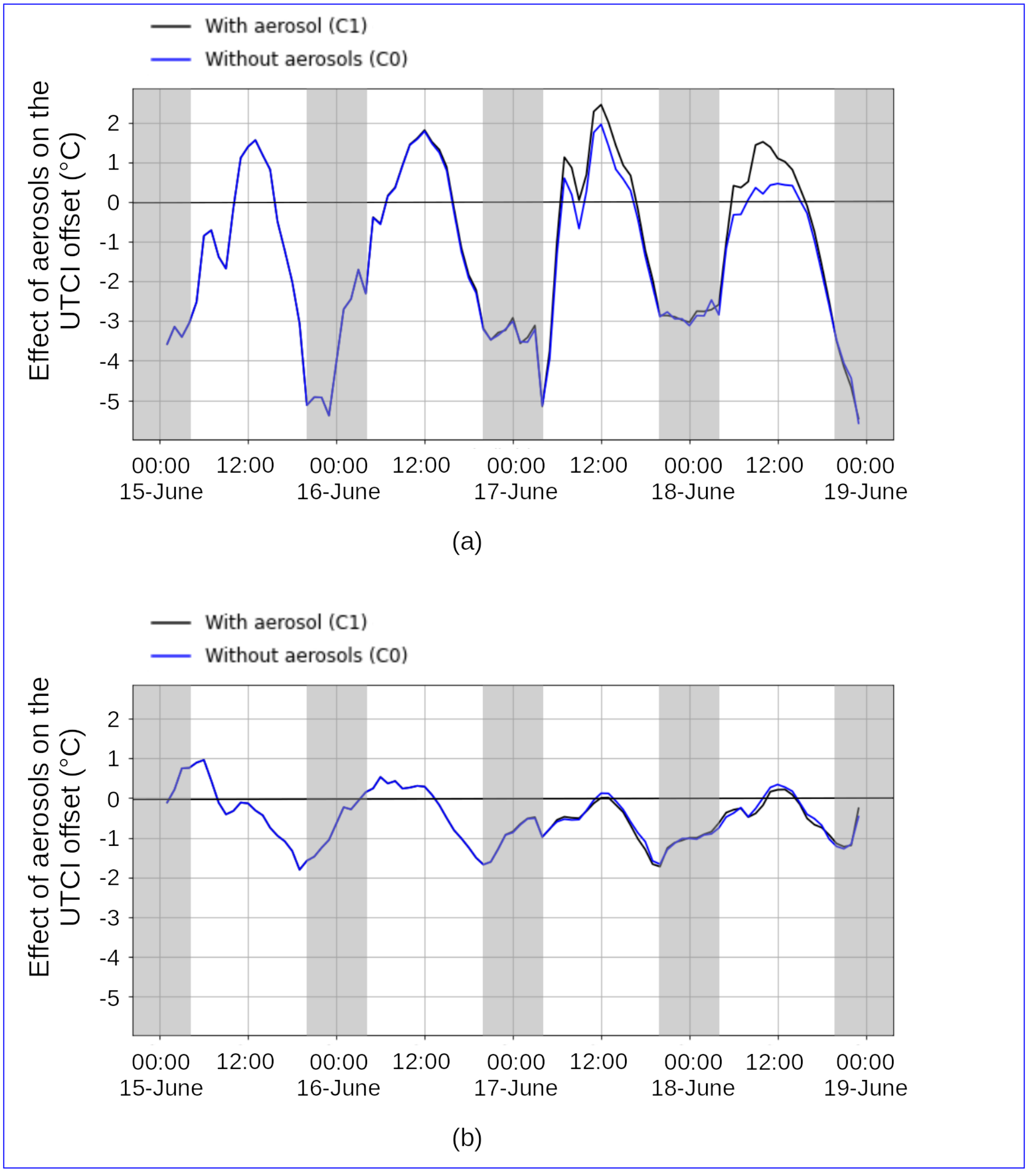


**Figure 13.** Temporal evolution from 15 to 18 June of the UTCI offset in the shade for (a) Palaiseau (suburbs) and (b) Lariboisière (city-center) locations, with and without dust aerosols (black and blue curves, respectively)

Figure 13 shows the temporal evolution from June 15 to June 18 of the UTCI offset in the shade ~~or in the sun, at~~ for the locations of Palaiseau (Fig. 13a) and Lariboisière ~~or Palaiseau ), the aerosols generally decrease the values of both air temperature and UTCI and therefore improve the thermal comfort when compared to the simulation without aerosol~~(Fig. 13b). No significant differences are found in the city-center between C0 and C1 simulations. However, ~~in the shade of sparsely built neighborhoods (Palaiseau~~while the aerosol plume passes over the Paris region (17 and 18 June), the UTCI offset ~~, which is the thermal comfort contribution of all variables except air temperature, is worse with aerosols than without aerosols,~~ increases substantially when explicitly considering dust, reaching a maximum ~~heating~~ difference between C1 and C0 simulations of up to 1.25°C at 10 ~~:00 UTC on 18 June (Fig. 13).~~

~~Temporal variation of the difference between UTCI in shade and air temperature for two sites for simulations C0 and C1~~

UTC on June 18. For that time, in Palaiseau, the differences in $T_{mrt}$, wind speed, and relative humidity between C1 and C0 are +1.5 °C, ~~-1~~ $-1$ m s$^{-1}$ and +3 %, respectively (not shown). These effects almost ~~compensated~~ compensate for the cooling due to the air temperature ~~reduction~~ mitigation and thus the presence of aerosol results in ~~an almost no~~ a negligible effect on thermal comfort (~~-0.2~~ $-0.2$ °C). Seen from a different perspective, ~~it also means that being in~~ in terms of thermal comfort for areas in the shade, the ~~shade in a suburban area with the~~ level of ~~aerosol observed on 18 June is equivalent, in terms of thermal comfort, to being in the shade with an aerosol-free atmosphere but with~~ dust aerosols observed on June 18 is equivalent to a 1.5 °C ~~higher~~ increase of air temperature.

To identify the contribution ~~$Contrib_i$~~ of each variable ~~$i$~~ to the effect of aerosols on UTCI (referred to as $Ct_\star$ with the indice $\star$ for the variable considered), the following calculation, illustrated in Eq. 2 with the variable $T_a$, is performed for $T_a$, $T_{mrt}$, $RH$, $U_{wind}$.

$$\text{~~Contrib~~}\,Ct_{T_a} = UTCI(T_{a_{C_1}}, U_{wind_{C_0}}, T_{mrt_{C_0}}, RH_{C_0}) - UTCI(T_{a_{C_0}}, U_{wind_{C_0}}, T_{mrt_{C_0}}, RH_{C_0}), \quad (2)$$

where the $C_0$ and $C_1$ subscripts refer to values in the C0 and C1 simulations.

Note that the full contribution of each variable can not be considered by this calculation, the UTCI equation defined by Jendritzky et al. (2012) having cross-contribution from each combination of two variables up to order 6. Thus, the sum of the individual contribution of each variable is not equal to the contribution of all variables at once, a residual term attributed to the cross-terms should be added (Eq. 3).

$$UTCI_{C_1} - UTCI_{C_0} = \text{~~Contrib~~}\,Ct_{T_a} + \text{~~Contrib~~}\,Ct_{U_{wind}} + \text{~~Contrib~~}\,Ct_{T_{mrt}} + \text{~~Contrib~~}\,Ct_{RH} + \text{~~Contrib~~}\,Ct_{cross-terms(T_a, U_{wind}, T_{mrt}, RH)} \quad (3)$$

Figure 14a shows the contribution of each meteorological variable to the effect of aerosols on UTCI ~~. For the Palaiseau site,~~ simulated on 18 June ~~at~~ for two locations (Lariboisière and Palaiseau) and two times of the day (10 ~~:00 UTC, apart from~~ and 16 UTC). For all combinations of locations and time, the air temperature ~~impacting the UTCI negatively (-1.5~~ is always the most impacted variable (from $-1.5$ °C ~~), all the variables contribute to increase the UTCI by~~ to $-0.5$ °C). Except for the Palaiseau station at 10 UTC, ~~0.4°C and 0.2°C for the wind speed,~~ the mean radiant temperature ~~and the relative air humidity, respectively. This relative contribution order is only observed for this specific time and location: for the rest of the situations~~is the second most impacted variable ($-0.3$ °C to $+0.4$ °C). At 10 UTC in Palaiseau, the effect of the ~~mean radiant temperature is larger in absolute value than the effect of wind speed and relative humidity (Fig. 14).~~ aerosols on the wind speed is considerable (from 3.1 m s$^{-1}$ in C0 it drops to 2.2 m s$^{-1}$ in C1), leading to a $+0.5$ °C contribution of the wind speed on UTCI value. The rest of the variables has a more limited impacts (absolute value lower than 0.2 °C) for the location and time considered. Note that for all situations investigated here, the cross-term contribution has a rather low value.

As previously observed in Fig. 13, on 18 June, the location (urban versus suburban) has a larger impact on the UTCI offset at 10 :00 UTC than at 16 :00 UTC: the effect of aerosol-induced reduction of UTCI is higher in Lariboisiere than in Palaiseau for any time of the day, but with greater importance with a larger contribution at 10 :00 (1.0 °C) than at 16 :00 UTC (0.5°C). In the afternoon, except for the mean radiant temperature, all variable contributions the contributions of all variables to UTCI are about the same for urban and suburban cases locations (Fig. 14b). Note that for all situations investigated here, the cross-term contribution has a rather low value.

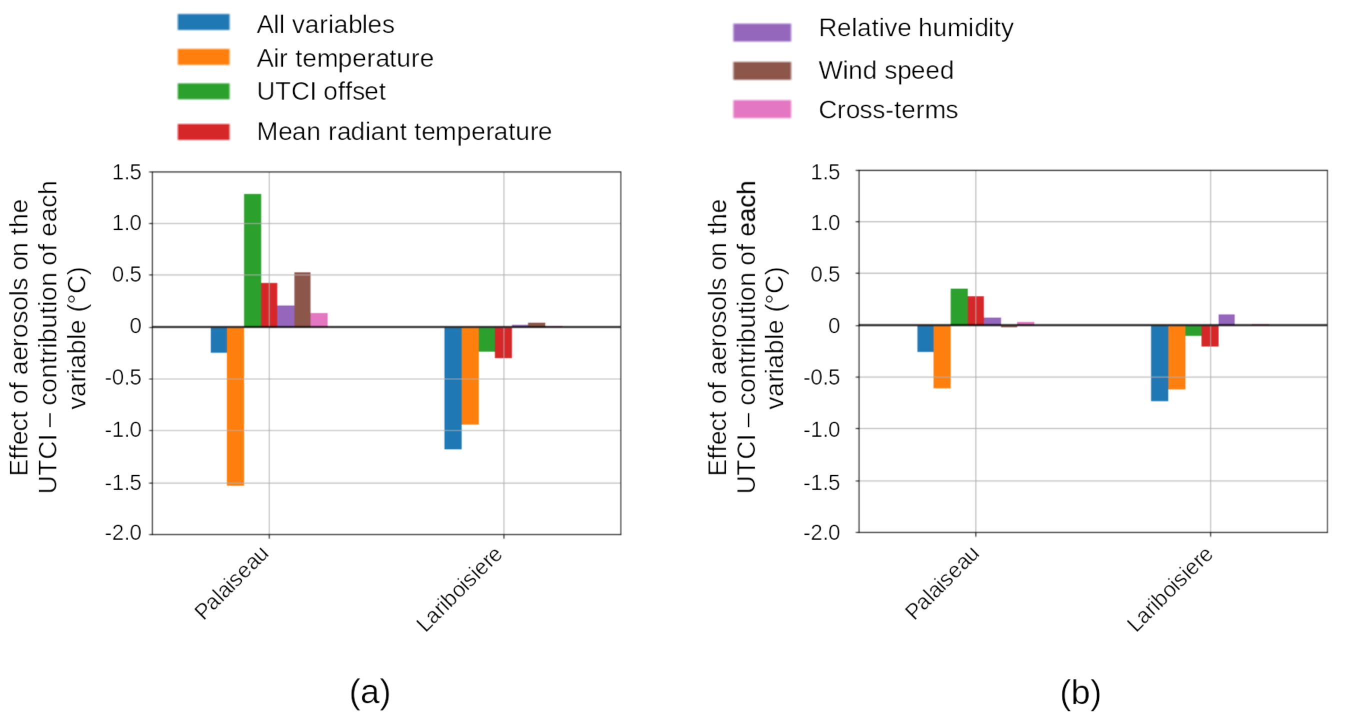


**Figure 14.** Contribution of all and each meteorological variable variables and cross-terms to the effect of aerosol on the UTCI on 18 June (a) at 10 :00 UTC and (b) at 16 :00 UTC

In summary, the presence of a dust plume during a heat wave contributes to reducing heatwave contributes to reduce global and direct solar radiation and air temperature, leading to improved improving human thermal comfort in sunlight, but no improvement in thermal comfort . However, it also increases diffuse solar radiation and generates a shallower boundary layer, inducing a slightly increased relative humidity and decreased wind-speed. Thus, the thermal comfort improvement under shade is consequently overall limited, and even negligible in suburban areasunder shade.

~~To assess the potential impact of dust aerosols on urban thermal comfort, a case of strong heatwave over the Paris region, associated with an inter-continental Saharan dust outbreak, is investigated. Simulations without and with dust aerosols are first validated against extensive observations of the PANAME-Urban experimental campaign. The simulations perform correctly~~

## 4 Discussion

In this study, we showed that dust aerosols significantly affected incident solar radiation leading to an overall attenuation of total radiation and a shift in the direct-to-diffuse ratio toward a larger diffuse component. These radiative effects have consequences on the dynamics of the atmospheric boundary layer, resulting in a decrease in surface air temperature, a slight increase in relative humidity and a slight decrease in wind speed. Such modifications have direct implications for human thermal comfort. Overall, the results ~~being consistent with observations, except the afternoon of the last day of the event being slightly overheated. This difference is mainly explained by the faster decrease of the AOD in the observations than in the simulations. Using the CAMS explicit dust aerosol fields in the simulations improves the results in all aspects. The impact of aerosols~~ of our work are consistent with previous studies that have documented aerosol impacts on meteorological variables and ABL processes, although some differences do emerge, particularly regarding thermal comfort.

per investigated the impact of ozone aerosol pollution on western Europe during the 2003 heatwave using offline-coupled WRF-CHIMERE simulations. Their results showed that aerosols increased AOD, reduced the mean solar radiation received at the surface by 15-30 W $m^{-2}$, and decreased the near-surface air temperature by approximately 0.3 °C. Aerosol-induced radiation and near-surface air temperature attenuation present geographical variations that can be explained by other influencing factors (properties and distribution of aerosols, or the response of surface fluxes to radiative forcing). This may explain why, in our case, despite comparable AOD values (approximately 0.6 on ~~incoming shortwave radiation is strong (up to a mean daily effect of -31 W/$m^2$)~~18 June 2022) and a similar reduction in solar radiation ($-32$ W $m^{-2}$), the decrease in near-surface air temperature was more important (1 °C). The absorption of solar radiation by aerosols is responsible for the heating of air in the ABL. Together with air cooling near the surface, this shrinks the ABL and enhances its stability -even above urban areas (**?**)- and weakens the near-surface wind speed (zha, a; per), a result also found in the present study.

In the urban environment, most studies have focused on fine anthropogenic aerosols and their influence on radiation and UHI. These studies consistently report a reduction in solar radiation during the day in urban areas, leading to ~~shallower boundary layers and cooler temperatures, both at ground level and within the atmospheric boundary layer~~a slight decrease ($-0.1$ °C) in the daytime air and surface UHI (**??**). At night, fine urban aerosols particles reduce the loss of longwave radiation from the surface (**?**) and therefore slightly increase the UHI (+0.12 °C, **?**) and the surface UHI (+0.5 °C, **?**). The impact ~~on thermal comfort is hence mainly driven by the air temperature, with improved thermal comfort sensation due to the dust aerosol impact. However, in the shadow of suburban areas(open low-rise neighborhoods) ,~~ of dust aerosols on UHI has been specifically investigated by **?** whom showed that, in semi-arid Chinese cities, coarse dust particles enhance surface UHI through increased longwave radiative forcing (up to +0.7 °C for an AOD increase of 0.13). In contrast, the ~~increased diffuse radiation, along with~~ surface UHI increase for cities located in humid or semi-humid climates was found to be negligible. Concerning our Paris study case, although dust aerosols were present over both urban and rural areas, no significant change in nighttime UHI intensity (difference between Lariboisiere and Palaiseau) was observed between aerosol and non-aerosol conditions. During daytime, the average UHI intensity was only marginally higher with aerosols (1.27 °C) than without (1.21 °C). This weak signal likely results from the spatial homogeneity of the dust plume, leading to negligible urban–rural AOD gradients, unlike in **?**.

Finally, the ~~lower wind speed and higher relative humidity, almost counterbalances the cooling effect due to air temperature.~~

~~While the total impact on thermal comfort is neutral for this specific area and meteorological event, this may be different under other conditions. Various factors and processes can influence this result, but the literature dedicated to~~ effect of aerosol on ~~thermal comfort is very limited. Obviously, the variability in radiative effects due to aerosol properties and distribution is a key component. But for a same AOD value, two events may have quite different radiationimpacts. Logothetis et al. have used the worldwide available AERONET data to highlight that for a same AOD value, the decrease in solar radiation at the bottom of the atmosphere is more important for fine particles than for coarse ones. Kaskaoutis et al. have also shown that the diffuse-direct irradiance ratio is higher for fine particles than for coarse particles. To determine the effect of aerosols on the other climate variables is even more complex. For example, the near-surface air temperature depends on the previously discussed incident solar flux but also on sensible and latent heat fluxes emitted by the terrestrial surface, on aerosol solar absorption near the ground and on atmospheric circulation (per). During the 7 to 15 August 2003 heat wave in Western Europe, a large amount of primary and secondary aerosols were emitted to the atmosphere and were associated to a large concentration of ozone. In the South of France, the mean solar radiation received at the surface was 30 W /m$^2$ lower than without aerosols, resulting in a 0.3 K decrease in near-surface air temperature (per). The same level of AOD (about 0.6~~ the radiative fluxes received by humans have been investigated, to the best of the author's knowledge, only once. **?** evaluated changes in mean radiant temperature across four East Asian cities for varying AOD conditions by coupling a radiative transfer model and a human thermal comfort model. Their results indicate that increasing AOD (from background levels of 0.1 to seasonal values between 0.4 and 0.9) leads to a higher $T_{mrt}$ at noon, mainly due to enhanced diffuse radiation. Although the AOD increases in their study is comparable to that observed in the present work (+0.5), our results differ: in our simulations, $T_{mrt}$ is lower in the presence of dust aerosols. A likely explanation is that, in our framework, aerosols influence not only solar radiation components but also air temperature, thereby affecting longwave radiation exchanges experienced by humans. In contrast, **?** considered only radiative effects.
During summertime and with high AOD value (AOD $>$ 1.4), their results show contrasting responses: AOD ranged between 1.4 and 1.8 led to substantial increases in $T_{mrt}$ and thermal stress in Chiayi and Hong-Kong, due to an increase in diffuse radiation, whereas very high AOD values (3.1-4) in Beijing and Seoul resulted in lower $T_{mrt}$ values due to strong attenuation of global radiation. Their analysis also highlights the influence of urban geometry: for all cities and conditions, $T_{mrt}$ at noon was consistently higher (by 1 °C) in their urban configuration (center of a 18 m wide (W = 18 m) street surrounded by 30 m height buildings (H = 30 m)) than in their open site reference (i.e without buildings or trees). This contrasts with our findings, where $T_{mrt}$ for a person standing in the sun on 18 June at noon is significantly higher in the more open site (Palaiseau) than

in the urban site (Lariboisière), both without aerosols (+4.46 °C) and with aerosols (+8.07 °C). These discrepancies may arise from differences in urban representation (idealized street canyon vs. building block arrays), as well as street orientation, surface albedo, material thermal properties and air temperature.

Despite these differences, both studies converge on a key point: aerosols, through their modulation of direct and diffuse solar radiation, significantly influence human thermal comfort. Depending on aerosol loading and environmental conditions, this could lead to situations where thermal comfort is improved due to the reduction of the total radiative flux, but also where it is negligible -or worsened in **?**- mainly due to the increase in diffuse solar radiation.

## 5 Conclusions

This study investigated the influence of a Saharan dust plume on urban thermal comfort during the June 15–19, 2022 ~~) and similar effect on the solar radiation (-32 W/m$^2$) were observed in our case, but the air temperature decrease was more important (~~heatwave in the Paris region, leveraging high-resolution atmospheric simulations (Meso-NH at 1.2 km) and observational data from the PANAME-Urban campaign. The results reveal that dust aerosols, with observed aerosol optical depth reaching 0.65 at its highest, substantially reduced incoming solar radiation by up to 75 $W\ m^{-2}$ and lower near-surface air temperatures by as much as 1 ~~K). In Spain, for the same 2003 heat wave event, the near surface air temperature decrease was the same as in Southern France (0.3 K) whereas the aerosol impact on solar radiationwas twice lower (-15 W/m$^2$). Thus a difference of location or period of the year, of aerosol type, size, concentration or aerosol distribution within the atmosphere level may lead to considerable differences on the four meteorological variables (air temperature, mean radiant temperature, wind speed~~ °C in sunlit urban and suburban areas, leading to measurable improvements in thermal comfort under direct sunlight. However, this radiative attenuation is accompanied by a 30 $W\ m^{-2}$ increase in diffuse radiation, a 1 $m\ s^{-1}$ reduction in wind speed, and a 0.4 $g\ kg^{-1}$ rise in specific humidity, which collectively counteracted the cooling effect in shaded suburban environments, resulting in negligible net changes in thermal comfort (differences of thermal comfort index close to zero between simulations using CAMS dust aerosols - C1 - and ~~air relative humidity) used to estimate the thermal comfort via the UTCI indicator~~no-dust - C0 - scenarios).

The ~~results presented in this study show that realistic consideration of atmospheric aerosols in weather forecasting models is essential for accurate prediction of heat exposure conditions in cities. In the present case study, certain insights into urban comfort conditions during desert dust plume events have been revealed. Nevertheless, the complexity of the radiation processes at play within the urban canopy and the feedbacks on local climate variables make it difficult to generalize these conclusions. Future work could study the influence of other types of aerosols on weather conditions and thermal comfort. This would be particularly relevant for aerosols emitted from cities inside the boundary layer. Another research direction could be to evaluate the impact of more intense dust episodes in cities nearby emission source areas, such as Athens in Greece, or Dakarin Senegal, both closer to the Sahara desert~~simulations demonstrated that incorporating dust aerosols from CAMS reanalysis improved the accuracy of meteorological predictions, particularly for solar radiation and air temperature, though biases persisted in boundary layer height simulations due to overestimated vertical mixing. The study also underscored the spatial variability of aerosol impacts: while urban centers experience a 1 °C UTCI reduction in sunlit areas, shaded suburban zones showed minimal improvement due to compensatory effects of humidity and wind speed.

While these findings are specific to a Saharan dust event, they provide a foundation for exploring the broader implications of aerosol-climate interactions in urban areas. Future research could extend this framework to cities closer to dust sources (e.g., Athens or Dakar), where aerosol optical depths frequently exceed 1.0, or to anthropogenic aerosols, which may exhibit different radiative and dynamic effects. Additionally, integrating these insights into operational heat-health warning systems—by coupling aerosol forecasts with bioclimatic indices like the UTCI—could enhance adaptive urban planning and public health responses during extreme heat events.

*Code and data availability.* The Meso-NH code is maintained and updated by CNRM and LAERO, and it is freely available for download at *https://zenodo.org/records/15095131* (**?**). Météo-France data such as RADOME observations, and AROME analyses and forecasts are available online at *https://meteo.data.gouv.fr/*. Raw observational data from the PANAME-Urban campaign are available from the AERIS data centre catalogue at *https://paname.aeris-data.fr/data-catalogue-2/*. The modified sources of the Meso-NH code, the configuration files and the CAMS data used to run the simulations are freely available for download at *https://zenodo.org/records/19374105*. Output data are available upon request.

*Author contributions.* JB has performed the simulations and analyses and contributed to all stages of the paper writing. TN performed the simulations, and contributed to the analyses and writing of the paper. VM coordinated the project proposal for CNRM, supervised the study, and contributed to the analyses and the writing of the paper. AL contributed to the analyses and reviewed the final draft of the paper. JW and QR provided support for the simulations and reviewed the final draft of the paper. PT contributed as expert in aerosols modeling and revised the final draft of the paper.

*Competing interests.* The authors declare that they have no conflict of interest.

*Acknowledgements.* We gratefully acknowledge the support and funding from the EU Action 2021-2-29 User-centric Assessment of Climate Change Impacts for Adaptation [U-CLIMADAPT] under Grant Agreement No 2022/SI2.879178 and SI2.879180/ SGA 20 implementing the FPA 275/G/GRO/COPE/17/10042. Numerical simulations have been undertaken on the Belenos HPC facility of Météo-France (Atos Bull Sequana with AMD Rome processors). We would like to thank Alejandra Velazquez-Garcia and Cyrielle Deanjean as well as Simone Kotthaus for the helpful discussions on dust transport and boundary layer height, respectively.

## References


The WMO SDS-WAS Regional Center for Northern Africa, Middle East and Europe, 99, https://doi.org/10.1051/e3sconf/20199904008.

Could aerosol emissions be used for regional heat wave mitigation?, 13, https://doi.org/10.5194/acp-13-6373-2013.

AERONET—A Federated Instrument Network and Data Archive for Aerosol Characterization, 66, https://doi.org/10.1016/S0034-4257(98)00031-5.

The AFWA dust emission scheme for the GOCART aerosol model in WRF-Chem v3.8.1, 12, https://doi.org/10.5194/gmd-12-131-2019.

Direct shortwave radiative forcing of the Asian dust aerosol on dust emission, 101, https://doi.org/10.1007/s00704-009-0245-3.

Impact of aerosol direct radiative forcing on the radiative budget, surface heat fluxes, and atmospheric dynamics during the heat wave of summer 2003 over western Europe: A modeling study.

Transport of Mineral Dust and Its Impact on Climate, 8, https://doi.org/10.3390/geosciences8050151.

Construction of the SILAM Eulerian atmospheric dispersion model based on the advection algorithm of Michael Galperin, 8, https://doi.org/10.5194/gmd-8-3497-2015.

Climate Change 2013. The Physical Science Basis. Working Group I Contribution to the Fifth Assessment Report of the Intergovernmental Panel on Climate Change - Abstract for decision-makers;

Roles of Atmospheric Aerosols in Extreme Meteorological Events: a Systematic Review, 8, https://doi.org/10.1007/s40726-022-00216-9.

Simulating chemistry–aerosol–cloud–radiation–climate feedbacks over the continental U.S. using the online-coupled Weather Research Forecasting Model with chemistry (WRF/Chem), 44, https://doi.org/10.1016/j.atmosenv.2010.05.056, a.

Strong Influence of Aerosol Reductions on Future Heatwaves, 46, https://doi.org/10.1029/2019GL082269, b.

Boone, A., Samuelsson, P., Gollvik, S., Napoly, A., Jarlan, L., Brun, E., and Decharme, B.: The interactions between soil–biosphere–atmosphere land surface model with a multi-energy balance (ISBA-MEB) option in SURFEXv8–Part 1: Model description, Geoscientific Model Development, 10, 843–872, 2017.

Brousseau, P., Seity, Y., Ricard, D., and Léger, J.: Improvement of the forecast of convective activity from the AROME-France system, Quarterly Journal of the Royal Meteorological Society, 142, 2231–2243.

Córdoba-Jabonero, C., Sicard, M., López-Cayuela, M.-, Ansmann, A., Comerón, A., Zorzano, M.-P., Rodríguez-Gómez, A., and Muñoz-Porcar, C.: Aerosol radiative impact during the summer 2019 heatwave produced partly by an inter-continental Saharan dust outbreak – Part 1: Short-wave dust direct radiative effect, Atmospheric Chemistry and Physics, 21, 6455–6479, https://doi.org/10.5194/acp-21-6455-2021, 2021.

Forster, A., Augros, C., and Masson, V.: Urban influence on convective precipitation in the Paris region: Hectometric ensemble simulations in a case study, Quarterly Journal of the Royal Meteorological Society, 150, 3028–3051, 2024.

Fouquart, Y.: Computations of solar heating of the Earth's atmosphere: A new parameterization, Beitraege zur Physik der Atmosphaere, 53, 35, 1980.

Hersbach, H., Bell, B., Berrisford, P., Biavati, G., Horányi, A., Muñoz Sabater, J., Nicolas, J., Peubey, C., Radu, R., Rozum, I., et al.: ERA5 hourly data on pressure levels from 1940 to present, Copernicus climate change service (c3s) climate data store (cds), 10, 24 381.

Hoarau, T., Barthe, C., Tulet, P., Claeys, M., Pinty, J.-P., Bousquet, O., Delanoë, J., and Vié, B.: Impact of the generation and activation of sea salt aerosols on the evolution of Tropical Cyclone Dumile, Journal of Geophysical Research: Atmospheres, 123, 8813–8831.

Hodnebrog, Ø., Myhre, G., Jouan, C., Andrews, T., Forster, P. M., Jia, H., Loeb, N. G., Olivié, D. J., Paynter, D., Quaas, J., et al.: Recent reductions in aerosol emissions have increased Earth's energy imbalance, Communications Earth & Environment, 5, 166, 2024.

Honnert, R., Masson, V., Lac, C., and Nagel, T.: A theoretical analysis of mixing length for atmospheric models from micro to large scales, Frontiers in Earth Science, 8, 582 056, 2021.

Inness, A., Ades, M., Agustí-Panareda, A., Barré, J., Benedictow, A., Blechschmidt, A.-M., Dominguez, J. J., Engelen, R., Eskes, H., Flemming, J., et al.: The CAMS reanalysis of atmospheric composition, Atmospheric Chemistry and Physics, 19.

Jendritzky, G., De Dear, R., and Havenith, G.: UTCI—why another thermal index?, International journal of biometeorology, 56, 421–428, 2012.

Kaskaoutis, D., Kambezidis, H., Dumka, U., and Psiloglou, B.: Dependence of the spectral diffuse-direct irradiance ratio on aerosol spectral distribution and single scattering albedo, Atmospheric Research, 178, 84–94.

Kotthaus, S., Haeffelin, M., Drouin, M.-A., Dupont, J.-C., Grimmond, S., Haefele, A., Hervo, M., Poltera, Y., and Wiegner, M.: Tailored Algorithms for the Detection of the Atmospheric Boundary Layer Height from Common Automatic Lidars and Ceilometers (ALC), Remote Sensing, 12, https://www.mdpi.com/2072-4292/12/19/3259, 2020.

Lac, C., Chaboureau, J.-P., Masson, V., Pinty, J.-P., Tulet, P., Escobar, J., Leriche, M., Barthe, C., Aouizerats, B., Augros, C., et al.: Overview of the Meso-NH model version 5.4 and its applications, Geoscientific Model Development, 11, 1929–1969, 2018.

Lemonsu, A., Barrau, S., Capo, J., Céspedes, J., Dahech, S., de Munck, C., Dumas, G., Jean-Charles, D., Dupuis, V., Etienne, J.-C., Garrouste, O., Goret, M., Haeffelin, M., Keravec, P., Kotthaus, S., Madelin, M., Martinet, P., Masson, V., Nagel, T., Price, J., Ribaud, J.-F., Rivollet, M., Roberts, G., Roy, A., Unger, V., Wilson, R., Wallois, S., and Wurtz, J.: PANAME-Urban campaign: investigating multiscale surface-atmosphere interactions and thermal-contrasts in the Paris region (France), Bulletin of the American Meteorological Society, pp. XX–XX, ~~under rev.~~in press.

Logothetis, S.-A., Salamalikis, V., and Kazantzidis, A.: The impact of different aerosol properties and types on direct aerosol radiative forcing and efficiency using AERONET version 3, Atmospheric Research, 250, 105 343.

Masson, V.: A physically-based scheme for the urban energy budget in atmospheric models, Boundary-layer meteorology, 94, 357–397, 2000.

Masson, V., Lemonsu, A., Hidalgo, J., and Voogt, J.: Urban climates and climate change, Annual Review of Environment and Resources, 45, 411–444.

Masson, V., Le Moigne, P., Martin, E., Faroux, S., Alias, A., Alkama, R., Belamari, S., Barbu, A., Boone, A., Bouyssel, F., et al.: The SURFEXv7. 2 land and ocean surface platform for coupled or offline simulation of earth surface variables and fluxes, Geoscientific Model Development, 6, 929–960, 2013.

Mlawer, E. J., Taubman, S. J., Brown, P. D., Iacono, M. J., and Clough, S. A.: Radiative transfer for inhomogeneous atmospheres: RRTM, a validated correlated-k model for the longwave, Journal of Geophysical Research: Atmospheres, 102, 16 663–16 682, 1997.

Noilhan, J. and Planton, S.: A simple parameterization of land surface processes for meteorological models, Monthly weather review, 117, 536–549.

Oke, T. R., Mills, G., Christen, A., and Voogt, J. A.: Urban climates, 2017.

Oke, T. R. et al.: Initial guidance to obtain representative meteorological observations at urban sites, vol. 81, 2004.

Pinty, J.-P. and Jabouille, P.: A mixed-phase cloud parameterization for use in mesoscale non-hydrostatic model: simulations of a squall line and of orographic precipitations, in: ~~Conf. on cloud physics~~Proceedings of the Conference of Cloud Physics, 17–21 August 1998. Boston MA, pp. 217–220, ~~Amer. Meteor. Soc. Everett, WA~~American Meteorological Society, 1998.

Redon, E., Lemonsu, A., and Masson, V.: An urban trees parameterization for modeling microclimatic variables and thermal comfort conditions at street level with the Town Energy Balance model (TEB-SURFEX v8. 0), Geoscientific Model Development, 13, 385–399, 2020.

Redon, E. C., Lemonsu, A., Masson, V., Morille, B., and Musy, M.: Implementation of street trees within the solar radiative exchange parameterization of TEB in SURFEX v8. 0, Geoscientific Model Development, 10, 385–411, 2017.

Rémy, S., Kipling, Z., Huijnen, V., Flemming, J., Nabat, P., Michou, M., Ades, M., Engelen, R., and Peuch, V.-H.: Description and evaluation of the tropospheric aerosol scheme in the Integrated Forecasting System (IFS-AER, cycle 47R1) of ECMWF, Geoscientific Model Development, 15, 4881–4912, https://doi.org/10.5194/gmd-15-4881-2022, 2022.

Riette, S.: Development of "Physical Parametrizations with PYthon"(PPPY, version 1.1) and its usage to reduce the time-step dependency in a microphysical scheme, Geoscientific Model Development, 13, 443–460.

Schoetter, R., Kwok, Y. T., de Munck, C., Lau, K. K. L., Wong, W. K., and Masson, V.: Multi-layer coupling between SURFEX-TEB-v9. 0 and Meso-NH-v5. 3 for modelling the urban climate of high-rise cities, Geoscientific Model Development, 13, 5609–5643, 2020.

Seity, Y., Brousseau, P., Malardel, S., Hello, G., Bénard, P., Bouttier, F., Lac, C., and Masson, V.: The AROME-France convective-scale operational model, Monthly Weather Review, 139, 976–991.

Skamarock, W. C., Klemp, J. B., Dudhia, J., Gill, D. O., Barker, D. M., Wang, W., and Powers, J. G.: A description of the advanced research WRF version 2, Tech. rep., NCAR, 2005.

Stewart, I. D. and Oke, T. R.: Local climate zones for urban temperature studies, Bulletin of the American Meteorological Society, 93, 1879–1900.

Tardieu, J. and Leroy, M.: Radome, le réseau temps réel d'observation au sol de Météo-France, La Météorologie, 40.

Tegen, I., Hollrig, P., Chin, M., Fung, I., Jacob, D., and Penner, J.: Contribution of different aerosol species to the global aerosol extinction optical thickness: Estimates from model results, Journal of Geophysical Research: Atmospheres, 102, 23 895–23 915, 1997.

Tulet, P., Grini, A., Griffin, R. J., and Petitcol, S.: ORILAM-SOA: A computationally efficient model for predicting secondary organic aerosols in three-dimensional atmospheric models, Journal of Geophysical Research: Atmospheres, 111, https://doi.org/https://doi.org/10.1029/2006JD007152.

Tulet, P., Mallet, M., Pont, V., Pelon, J., and Boone, A.: The 7–13 March 2006 dust storm over West Africa: Generation, transport, and vertical stratification, Journal of Geophysical Research: Atmospheres, 113, 2008.

Wiki – CNRM: Wiki – ECOCLIMAP-SG – CNRM Open Source Site. Retrieved from *https://opensource.umr-cnrm.fr/projects/ecoclimap-sg/wiki*. Accessed 20 february 2025., 2018.

Wurtz, J., Bouniol, D., and Vié, B.: Improvements to the parametrization of snow in AROME in the context of ice crystal icing, Quarterly Journal of the Royal Meteorological Society, 2023.